

# Extremal isosystolic metrics with multiple bands of crossing geodesics

Usman Naseer<sup>1,2,3</sup> and Barton Zwiebach<sup>3</sup>

<sup>1</sup>*Department of Physics,  
Harvard University,  
Cambridge, MA, 02138, USA*

<sup>2</sup>*Department of Physics and Astronomy,  
Uppsala University,  
Box 516, SE-751s 20 Uppsala, Sweden*

<sup>3</sup>*Center for Theoretical Physics  
Massachusetts Institute of Technology  
Cambridge MA 02139, USA*

unaseer@g.harvard.edu, zwiebach@mit.edu

## Abstract

We apply recently developed convex programs to find the minimal-area Riemannian metric on  $2n$ -sided polygons ( $n \geq 3$ ) with length conditions on curves joining opposite sides. We argue that the Riemannian extremal metric coincides with the conformal extremal metric on the regular  $2n$ -gon. The hexagon was considered by Calabi. The region covered by the maximal number  $n$  of geodesics bands extends over most of the surface and exhibits positive curvature. As  $n \rightarrow \infty$  the metric, away from the boundary, approaches the well-known round extremal metric on  $\mathbb{RP}_2$ . We extend Calabi's isosystolic variational principle to the case of regions with more than three bands of systolic geodesics. The extremal metric on  $\mathbb{RP}_2$  is a stationary point of this functional applied to a surface with infinite number of systolic bands.

# Contents

<b>1</b>	<b>Introduction</b>	<b>2</b>
<b>2</b>	<b>Riemannian and conformal metrics with dihedral symmetry</b>	<b>5</b>
2.1	The polygons and the curves to be constrained . . . . .	5
2.2	Riemannian and conformal metrics on $P_{2n}$ . . . . .	7
<b>3</b>	<b>Convex programs for conformal metrics on polygons</b>	<b>8</b>
3.1	Primal Program . . . . .	8
3.2	Dual Program . . . . .	10
3.3	Edge length and height parameter . . . . .	13
<b>4</b>	<b>Calabi's hexagon</b>	<b>16</b>
4.1	Setup for convex programs . . . . .	16
4.2	Numerical results, metric description, and consistency checks . . . . .	18
<b>5</b>	<b>The cases of the octagon and decagon</b>	<b>21</b>
5.1	Setup for the convex programs . . . . .	22
5.2	Numerical results and patterns of bands . . . . .	23
5.3	The decagon briefly noted . . . . .	25
<b>6</b>	<b>Higher polygons and the extremal metric on <math>\mathbb{RP}_2</math></b>	<b>26</b>
6.1	Riemannian and conformal extremal metrics on $\mathbb{RP}_2$ . . . . .	27
6.2	Area, perimeter, and metric for large $n$ polygons . . . . .	29
<b>7</b>	<b>Conformal metric on <math>\mathbb{RP}_2</math> from the dual program</b>	<b>31</b>
7.1	Setting up the calculation . . . . .	31
7.2	Working out the details . . . . .	32
<b>8</b>	<b>Calabi's variational principle</b>	<b>38</b>
8.1	The variational principle for regions with three systolic bands . . . . .	38
8.2	Connecting the conformal and isosystolic formalisms . . . . .	39
8.3	Comments on a suggested extension for multiple bands . . . . .	41
<b>9</b>	<b>Isosystolic variational principle with multiple foliations</b>	<b>44</b>
9.1	Extension of the variational principle . . . . .	44
9.2	Extremal Riemannian metric on $\mathbb{RP}_2$ from new variational principle . . . . .	45
<b>A</b>	<b>Discretization of polygons for numerical analysis</b>	<b>49</b>
A.1	Hexagon . . . . .	49
A.2	Octagon and higher polygons . . . . .	50

# 1 Introduction

The subject of minimal area *conformal* metrics on Riemann surfaces is an old one (see, for example, [1, 2]). Sometimes called extremal length problems, they ask for the conformal metric of least area on a fixed Riemann surface under some length conditions. Typically the length conditions require that certain sets of curves have length bounded below by some fixed constants. In order to find the string diagrams that would define a closed string field theory a minimal area problem on (punctured) Riemann surfaces was proposed in which a single length condition applies to *all* non-contractible closed curves on the surface [3–5]. All such curves must be longer than the *systole*  $\ell_s$ , a number that can be conventionally set equal to one, or  $2\pi$ , or any fixed constant.

Consider this conformal minimal area problem for the case of a Riemann surface of genus  $g$  with no punctures. In general the extremal metric is not known. In genus  $g$  we have a moduli space  $\mathcal{M}_g$  of Riemann surfaces. For string field theory we need the minimal area metric for each point on  $\mathcal{M}_g$ , that is, for each and every Riemann surface of genus  $g$ . If we knew these extremal metrics and their area we could ask for those Riemann surfaces for which the extremal area is a minimum over the moduli space. Those surfaces would be solutions of the problem of finding the *Riemannian* metric of least area on a genus  $g$  surface under the same length condition. Indeed, as we vary over the space of Riemannian metrics we change the complex structure, and in this way we end up finding the Riemann surface (or surfaces) that has the least area. This problem of extremal Riemannian metrics has been investigated in Gromov [6] and is a problem of systolic geometry [7–9]. The conformal specialization has also been explored in [10]. The case of metrics with non-positive curvature has been studied in [11, 12].

It is clear that on two-dimensional surfaces the conformal minimal area problem is richer than the Riemannian version. In fact, extremal conformal metrics show different behavior. While conformal minimal-area metrics can have regions where there is exactly one band of systolic geodesics [1, 4], Riemannian extremal metrics cannot, as explained by Calabi [13]. In Riemannian extremal metrics regions with exactly two bands of geodesics are flat and the geodesics are orthogonal [13]. In the conformal version, as was recently discovered [14, 15], regions with two bands of geodesics support positive and sometimes negative curvature.

Indeed, recent work with M. Headrick [14, 15] applied the methods of convex optimization [16] to the conformal minimal area problem. The result was a couple of programs, a primal and its dual, that give new analytic insights into the form of the minimal area metrics. Additionally, they can be used to find accurate minimal area metrics and to deal with the minimal area problem of string field theory. The dual program involves the maximization of a functional. Its optimum, by the property of strong duality, coincides with the minimum of the primal.

In this paper we explore a set of issues motivated by the work of Calabi [13]. He considered a regular hexagon in  $\mathbb{R}^2$  and asked for the Riemannian metric of least area under the condition that all curves joining opposite sides of the hexagon be longer than or equal to one. Reference [13] assumes that the metric is unique and thus admits the dihedral group  $D_6$  of symmetries as isometries. We will consider this problem in detail, as well as the obvious generalization to regular  $2n$ -sided polygons  $P_{2n}$ , with  $n \geq 3$ . We visualize these regular polygons as regions of the complex  $z$  plane. We claim that the minimal area *Riemannian* metric on  $P_{2n}$ , if unique, is in fact the minimal area *conformal* metric on  $P_{2n}$ . The argument is presented in section 2.2. It follows that we can use the methods of [14, 15] to study the problem posed by Calabi as well as its generalization to higher polygons.

Calabi also proposed a variational principle for the metric, valid for regions with exactly three bands of systolic geodesics. This was studied further in [17], who gave more details on the differential equations arising from the variational principle and following [13] proposed an extension to regions covered by more than three bands of systolic geodesics. We have found difficulties with this proposal and have constructed a new variational principle to circumvent these difficulties.

For the case of the hexagon we confirm that there is a large central region  $U_3$  covered by three bands of geodesics, and a region  $U_2$  comprising neighborhoods of the vertices that are flat and are covered by two orthogonal bands of geodesics (see Figure 8). A Gauss-Bonnet argument shows that the integral of the Gaussian curvature over  $U_3$  is equal to  $2\pi$ , the amount that corresponds to half a sphere. We find an accurate estimate of the extremal area using the primal and dual programs.<sup>1</sup> Moreover, the methods of [14] give an exact relation  $\mathcal{P} = 4A/\ell_s$  between the perimeter  $\mathcal{P}$  of the polygon and its area  $A$  in the minimal area metric with systole  $\ell_s$ .

Since the possible behavior of metrics in regions covered by multiple bands of systolic geodesics is of great interest, higher polygons are a natural ground for exploration. A polygon  $P_{2n}$  is expected to have a region  $U_n$  with precisely  $n$  systolic geodesics going through every point. For the case of an octagon we find a rather large central region  $U_4 \in P_8$  (see Figure 9). There are also small regions  $U_3$  and  $U_2$ . We find strong evidence that the integral of the Gaussian curvature over  $U_4$  is equal to  $2\pi$ . We briefly discuss the 10-gon or decagon. For this polygon we find strong evidence that the integral of the Gaussian curvature over  $U_5$  is equal to  $2\pi$ , in contradiction with the claim [17] that the extremal metric in regions  $U_k$  with  $k \geq 5$  must be flat (see Figure 11).

We observe that the region  $U_n \subset P_{2n}$  covered by  $n$  bands fills a larger part of  $P_{2n}$  as  $n$  increases, and the integrated curvature over  $U_n$  remains constant at  $2\pi$ . These patterns make sense in the limit of very large  $n$ . We find evidence that, away from the boundary of the polygon, the minimal area metric on  $P_{2n}$  approaches the minimal area Riemannian metric on  $\mathbb{RP}_2$  as  $n \rightarrow \infty$ . This metric was obtained by Pu [18]. It takes the form of a constant-curvature hemisphere, whose boundary is subject to antipodal identifications. We can view this metric as one with infinite number of geodesic bands, each band defined by a pair of antipodal points on the boundary prior to identification. Each geodesic band covers the full hemisphere and the integrated curvature is indeed  $2\pi$ . The conformal version of the minimal area metric on  $\mathbb{RP}_2$  has also been studied. This problem asks for the minimal area conformal metric on a disk  $|z| \leq \frac{1}{2}$  with the condition that any curve going from a point to its antipode is of length larger than or equal to one. Reference [2] shows that the extremal metric is indeed the constant curvature metric that makes the disk into a hemisphere. This is, of course, the same exact metric that Pu found, showing that in this case the Riemannian and conformal problems are the same, just as we believe they are for all polygons  $P_{2n}$ .

The extremal metric on  $P_{2n}$  approaches the hemisphere metric except at the boundary, where the discrete nature of the problem appears to make a difference. The perimeter/area relation  $\mathcal{P} = 4A/\ell_s$ , valid for all polygons  $P_{2n}$ , does not hold for the hemisphere metric where we have instead  $\mathcal{P} = \pi A/\ell_s$ . In fact, each corner of the polygon has a flat neighborhood  $U_2$  with the two incident edges meeting orthogonally. This makes the metric diverge in the original coordinates where incident edges meet with angles approaching  $\pi$  as  $n \rightarrow \infty$ . We have some sort of infinitely ‘serrated’ boundary. More work will be needed to find the detailed picture of the metric near the boundary. We also do not know much about line curvature singularities of the metric as well as the curvature in the rapidly shrinking  $U_{n-1}, \dots, U_2$  regions.

---

<sup>1</sup>It is not clear from [13] if the differential equations relevant to the problem were studied numerically.

We then examine the dual functional of [14] for the extremal metric on  $\mathbb{RP}_2$ . Here the challenge is to show that this metric provides the optimum of the functional. Each band, parametrized by the value  $\phi_0$  of the azimuth of the starting point (and azimuth  $\pi + \phi_0$  for the ending point) provides a local coordinate system with coordinates  $x_{\phi_0}$  measuring length along the geodesics and  $\varphi_{\phi_0}$  which is a constant along each geodesic. Since the geodesics are known,  $\varphi_{\phi_0}$  is determined up to reparameterization. There is one key constraint following from the dual functional. The equation

$$\sum_{\phi_0} |d\varphi_{\phi_0}| = 1, \quad (1.1)$$

must hold at *every* point of the sphere. This is not easily satisfied since every candidate  $\varphi_{\phi_0}$  is a nontrivial function on the sphere. Moreover, the sum must be turned into an integral. We found the solution  $\varphi_{\phi_0}(\theta, \phi)$  satisfying this condition and showing that the extremal metric is the optimum of the dual program.

The metric on  $\mathbb{RP}_2$  also allows us to test the variational principle of [13, 17]. We use two bands of geodesics on the extremal metric to introduce coordinates  $X, Y$  on the sphere. A third, arbitrary band, is fixed by a pair of antipodal points and defines a length-based coordinate  $Z(X, Y)$ . The least-area variational principle in [13, 17] gives a partial differential equation for  $Z$ . Unfortunately, the equation is *not* satisfied. We propose a modification of Calabi's variational principle for regions with three or more bands of geodesics. The new proposal uses Lagrange multipliers to impose the constraints on the norm of one-forms that arise from each geodesic band. The equations of motion are nontrivially modified. We then show that the extremal metric on  $\mathbb{RP}_2$  is a solution for the equations following from the new variational principle.

Here is a summary of our main results:

1. Showing (up to a uniqueness assumption) that the Riemannian and conformal minimal area metrics are the same for polygons  $P_{2n}$ ,  $n \geq 3$ , with dihedral symmetry (section 2.2).
2. Finding an extension of Calabi's isosystolic variational principle valid for regions  $U_m$  covered by  $m \geq 3$  bands of systolic geodesics (section 9.1).
3. Showing that the extremal metric on  $\mathbb{RP}_2$  is a solution of the dual conformal program (section 7) as well as a solution of the new isosystolic variational principle (section 9.2).
4. A study of extremal metrics on  $P_{2n}$  with  $n \geq 3$  showing the interplay of multiple bands of geodesics and suggesting convergence for  $n \rightarrow \infty$  to the extremal  $\mathbb{RP}_2$  metric away from the boundary (section 6).

This paper is organized as follows. In section 2 we define the minimal area problem on polygons and establish that the Riemannian and conformal problems are equivalent. In section 3 we discuss the explicit formulation of the primal and dual programs for arbitrary regular polygons  $P_{2n}$ . The dual program has a height parameter  $\nu$  which is fixed at the optimum. This parameter determines the extremal area via the formula  $A = n\nu\ell_s^2$ . We show that this parameter also determines the length  $L_e$  of each edge of the polygon via the formula  $L_e = 2\nu\ell_s$ . This allows one to establish the perimeter/area relations discussed above.

Section 4 gives our results for Calabi's hexagon. We provide a detailed accounting of the curvature on the surface, which includes negative curvature on the boundary of  $U_3$ . The critical area

$A = 0.840$  is only about 3% lower than the area of the admissible flat-metric on the hexagon. The pattern of systolic geodesics on the surface is shown in Figure 8. Section 5 deals with the case of the octagon and then briefly the decagon, discussing the curvature on their central regions.

In section 6 we review the extremal metric on  $\mathbb{RP}_2$  [18], setting up the notation to compare it with the extremal metric on  $P_{2n}$  for large  $n$ . We show numerical evidence of convergence of the metric to the  $\mathbb{RP}_2$  metric as long as we are away from the boundary. In section 7 we show that the extremal metric on  $\mathbb{RP}_2$  is in fact the optimum for the variational system defining the dual program of [14]. This is a rather nontrivial test of dual program and provides further evidence of the claimed relation of the polygonal problem to the  $\mathbb{RP}_2$  problem in the limit  $n \rightarrow \infty$ .

In section 8 we review the variational approach of Calabi [13] explaining the introduction of potentials associated to (two) systolic bands, that serve as coordinates on the surface, and the description of the area form using the potential for yet another systolic band. We review the variational principle, and write down the explicit form of the equation of motion. We use the  $\mathbb{RP}_2$  metric to show that the equations of motion must be changed to deal with more than three bands of systolic geodesics. In section 9 we give the isosystolic variational principle valid in regions with three or more bands of systolic geodesics. We confirm that the extremal metric on  $\mathbb{RP}_2$  is a stationary point of the new functional.

## 2 Riemannian and conformal metrics with dihedral symmetry

In this section we begin by defining the regular  $2n$ -gon  $P_{2n}$  as a region of the complex plane. After describing the sets of curves whose lengths are constrained, we define conformal and Riemannian versions of the minimal area problem. Assuming the Riemannian problem has a unique solution we show that it coincides with the solution of the conformal problem.

### 2.1 The polygons and the curves to be constrained

We will consider regular  $2n$ -gons with  $n \geq 3$  and will present them as a region  $P_{2n}$  on the  $z = x + iy$  plane with the center at the origin and with two opposite edges orthogonal to the  $x$  axis at  $x = \pm \frac{1}{2}$ , each bisected by the axis (see Figure 1). The polygons so defined have apothem equal to  $\frac{1}{2}$ . There are  $n$  sets of curves,  $C_1, \dots, C_n$ , that are constrained in this polygon. These are the curves that join opposite edges of the polygon. A typical curve starts at any point on one edge and ends at an arbitrary point on the *opposite* edge. With the fiducial distance between edges equal to one, it is convenient to set the systole length  $\ell_s$  equal to one. In the chosen presentation we take  $C_1$  to be the curves that run between the opposite edges that intersect the  $x$  axis; the edge  $e_1$  at  $x = -\frac{1}{2}$  and the edge  $\tilde{e}_1$  at  $x = \frac{1}{2}$ . The curves on  $C_2$  are obtained by a rotation of  $\pi/n$  applied to the curves on  $C_1$ ; they begin on  $e_2$  and end on  $\tilde{e}_2$ . The curves on  $C_\alpha$ , with  $1 < \alpha \leq n$  are obtained by a rotation of  $(\alpha - 1)\pi/n$  applied to the curves on  $C_1$ . They begin on  $e_\alpha$  and end on  $\tilde{e}_\alpha$ . The polygon  $P_{2n}$  is invariant under transformations of the dihedral group  $D_{2n}$ . These are generated by rigid rotations by  $\pi/n$  and reflections about any line joining the midpoints of two opposite edges.

For the conformal minimal area problem we search in the space of metrics conformal to the fiducial metric  $|dz|^2$ . Because of convexity of the conformal problem, the dihedral transformations must be isometries of the extremal metric and we can therefore restrict ourselves to search over the space of metrics on  $P_{2n}$  with such symmetry. This also means that we know the metric over the

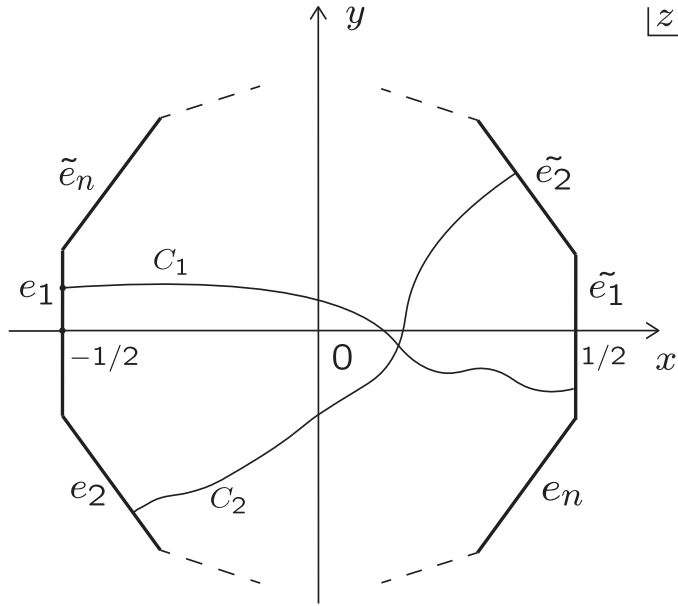


**Figure 1:** The canonical presentation of the  $2n$ -gon  $P_{2n}$  on the  $z$  plane, with center at the origin and with opposite edges  $e_1$  and  $\tilde{e}_1$  bisected orthogonally by the real line at the points  $x = \pm\frac{1}{2}$ . The curves starting on  $e_1$  and ending on  $\tilde{e}_1$  belong to the class  $C_1$ . After a rotation of a curve on  $C_1$  by an angle  $\pi/n$  we obtain a curve in  $C_2$ , starting on  $e_2$  and ending on  $\tilde{e}_2$ .

whole polygon if we know it on the fundamental domain of the dihedral transformations. We can choose the fundamental domain to be the right triangle  $T_{2n}$  with a vertex at the origin, the second vertex at  $(\frac{1}{2}, 0)$  and the third vertex at the polygon corner above  $x = \frac{1}{2}$  (see Figure 2).

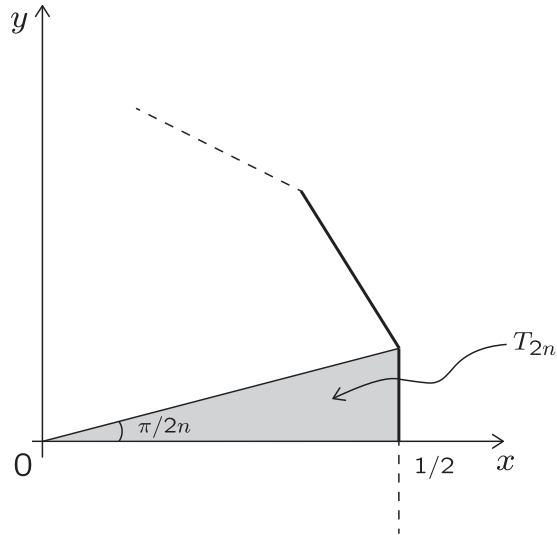


**Figure 2:** The right triangle  $T_{2n}$  in the polygon  $P_{2n}$  is a fundamental domain for the extremal metric. If known on  $T_{2n}$  the metric can be extended to  $P_{2n}$  using the dihedral isometries.

The fiducial metric  $g_{\mu\nu}^0$  on the polygon is taken to be the constant unit metric in the  $z$  plane:

$$g_{\mu\nu}^0 dx^\mu dx^\nu = dx^2 + dy^2. \quad (2.1)$$

It follows that the fiducial area form  $\omega_0$  is

$$\omega_0 = d^2x\sqrt{g^0} = dxdy. \quad (2.2)$$

The general conformal metric on the polygon takes the form

$$g_{\mu\nu} = \Omega g_{\mu\nu}^0, \quad (2.3)$$

with  $\Omega$  a function on the polygon. The area form  $\omega$  is then

$$\omega = d^2x\sqrt{g} = \Omega dxdy. \quad (2.4)$$

The area of  $P_{2n}$  is  $\int_{P_{2n}} dxdy\Omega$ . Parameterizing a closed curve  $\gamma$  using  $x^\mu(t) : [0, 1] \rightarrow P_{2n}$ , we have  $\text{length}(\gamma) = \int_\gamma \sqrt{\Omega} |\dot{x}|_0$ , where  $|\cdot|_0$  denotes norm in the fiducial metric.

In the Riemannian version of the problem not much is changed. The polygon  $P_{2n}$  is presented the exactly the same way, and the set of curves to be constrained are exactly the same. The metrics, however, are no longer required to be conformal to the fiducial metric; they are arbitrary. Lacking a convexity property it seems challenging to show that the extremal metric is unique, and therefore, just as in [13], we will assume it is. In this case, the extremal metric must be invariant under the dihedral group  $D_{2n}$ .

## 2.2 Riemannian and conformal metrics on $P_{2n}$

Consider the Riemannian minimal area problem on the regular polygon  $P_{2n}$ , presented as a region of the  $z$  plane. We will assume that the extremal metric  $g^0$  is unique and therefore has the dihedral symmetry  $D_{2n}$  of the polygon as isometries. We want to show that  $g^0$  defines the canonical conformal structure on  $P_{2n}$  or, equivalently,  $g^0$  is conformal to the flat metric  $|dz|^2$  on  $P_{2n}$ .

Here are the steps that allow us to reach this conclusion.<sup>2</sup>

1. The conformal structures for a  $2n$ -gon can be represented as a round disk  $|w| \leq 1$  with labeled marked points on the boundary corresponding to the vertices. Alternatively, they can be represented as the upper half plane  $\text{Im } w > 0$ , with boundary the real line, and marked points on the boundary. Since the positions of three marked points can be fixed at will by conformal maps, for a  $2n$ -gon, the conformal moduli space  $\mathcal{M}_{2n}$  is of real dimension  $2n - 3$ .

The moduli space can also be defined as the space of Riemannian metrics on  $P_{2n}$  modulo diffeomorphisms (keeping the boundary and vertices unchanged) and Weyl transformations. Any metric  $g$  on  $P_{2n}$  defines a conformal structure  $\lambda(g) \in \mathcal{M}_{2n}$ .

2. Now consider the action of the dihedral group on any metric  $g$  on  $P_{2n}$  and focus on the rotation subgroup, generated by the transformation  $Q : z \rightarrow ze^{i\pi/n}$  satisfying  $Q^{2n} = 1$ . Note that  $Q$  cycles the vertices and  $2n$  is the smallest possible integer for which  $Q$  raised to this power gives the identity. We can think of  $Q$  as an active transformation that rotates the metric by  $\pi/n$  while keeping the labeling of the punctures the same. We write  $Q : g \rightarrow Q(g)$ . It follows that this induces an action on the moduli space  $\mathcal{M}_{2n}$  as  $Q : \lambda(g) \rightarrow \lambda(Q(g))$ . If the metric  $g$  is dihedral invariant, it is also rotational invariant and  $\lambda(g)$  is a fixed point of the action of  $Q$  on the moduli space.

---

<sup>2</sup>We thank M. Headrick for his help in constructing this argument.



Any action of  $Q$  on the moduli space that leaves a point  $\lambda \in \mathcal{M}_{2n}$  invariant is in fact leaving a Riemann surface invariant and thus must be realized by a conformal map, in this case, a projective transformation  $\tilde{Q}$ . This projective transformation must be such that  $\tilde{Q}^{2n}$  is the identity transformation and no lower power of  $\tilde{Q}$  is the identity.

3. We now claim that a unit disk  $R_{2n}$  with  $2n$  marked points admitting a nontrivial conformal self map  $\tilde{Q}$  such that  $\tilde{Q}^{2n}$  is the lowest power of  $\tilde{Q}$  equal the identity is conformal to the unit disk with the  $2n$  marked points equally spaced along the boundary of the disk.

For this we present a disk  $R_{2n}$  on the upper half-plane  $H = \text{Im } u \geq 0$  with boundary the real line and marked points on the boundary. The generator  $Q$  of rotational symmetry cycling the  $2n$  marked points must be implemented as a projective transformation  $u \rightarrow \tilde{Q}(u)$ , which must satisfy  $\tilde{Q}^{2n} = \mathbf{1}$ . Projective transformations come in three types: hyperbolic, parabolic, and elliptic. A hyperbolic transformation has two fixed points on the real line. By conjugation with another projective transformation the two fixed points can be placed at 0 and at  $\infty$ , and then the transformation acts like  $u \rightarrow cu$  with  $c$  a real positive number. Such a transformation, if nontrivial ( $c \neq 1$ ), cannot have its  $2n$ -th power equal to the identity. So  $\tilde{Q}$  cannot be hyperbolic. It cannot be parabolic either, for a parabolic transformation has a single fixed point, which can be placed at  $\infty$  making the transformation take the form  $u \rightarrow u + b$  for  $b$  real and nonzero. Such a transformation cannot have its  $2n$ -th power equal to the identity. The transformation  $\tilde{Q}$  must therefore be elliptic. Elliptic transformations have two fixed points  $\eta$  and  $\eta^*$ , one the complex conjugate of the other. The map  $B : u \rightarrow w$  of  $u \in H$  to the unit disk  $|w| < 1$  is given by

$$w = \frac{u - \eta}{u - \eta^*}. \quad (2.5)$$

It follows that  $w = 0$  is a fixed point of  $\hat{Q} = B\tilde{Q}B^{-1}$ . A map of a round disk to itself preserving the origin must take the form  $w \rightarrow we^{i\theta}$ , and the condition  $\tilde{Q}^{2n} = \hat{Q}^{2n} = \mathbf{1}$  implies  $w \rightarrow we^{i2\pi/n}$ . This shows that the disk  $R_{2n}$  can be presented as the unit disk with equally spaced  $2n$  marked points. This is what we wanted to show.

4. Having identified a *unique* point in the moduli space with  $Q$  action invariance, it follows that any dihedral invariant metric  $g$  corresponds to this point on moduli space. The point is also the image of the canonical flat metric  $|dz|^2$  on  $P_{2n}$ . This completes our proof.

### 3 Convex programs for conformal metrics on polygons

We now give the explicit formulation of the primal and dual convex programs that determine the extremal conformal metric on the regular polygons  $P_{2n}$ . By the result of section 2.2 this extremal conformal metric is also the Riemannian extremal metric. For a detailed explanation of these primal and dual programs see [14], for a brief review see [15]. The dual program height parameter  $\nu$ , fixed at the optimum, determines the extremal area via  $A = n\nu\ell_s^2$ . We then prove that  $\nu$  also determines the length  $L_e$  of each edge of the polygon via  $L_e = 2\nu\ell_s$ .

#### 3.1 Primal Program

The primal program makes use of calibrations, one for each class  $C_k$  of curves on the Riemann surface. The calibrations are closed one forms with some specified periods and with norm less than

or equal to one. The norm is defined with respect to the conformal metric on the surface. The calibrations  $u^\alpha$  take the form

$$u^\alpha = \omega^\alpha + d\phi^\alpha, \quad (3.1)$$

where  $\omega^\alpha$  is a one-form with the requisite periods for the curves  $C_\alpha$  and the function  $\phi^\alpha$  defines the trivial part of the calibration. The first calibration  $u^1$  associated with  $C_1$  is given by

$$u^1 = dx + d\phi^1. \quad (3.2)$$

The choice  $\omega^1 = dx$  is consistent in that, as required,

$$\int_{\gamma \in C_1} dx = 1. \quad (3.3)$$

As discussed for the case of the Swiss cross or the torus [15], the symmetry of this calibration under  $(x, y) \rightarrow (x, -y)$  implies there is no contribution to  $\omega^1$  from  $dy$ . Since the integral  $\int d\phi^1$  over any curve in  $C_1$  must vanish, the value of  $\phi^1$  on  $e_1$  must be a constant equal to the value of  $\phi^1$  on  $\tilde{e}_1$ . We can choose this value to be zero:

$$\phi^1 \Big|_{e_1} = \phi^1 \Big|_{\tilde{e}_1} = 0. \quad (3.4)$$

Since the polygon is symmetric under reflections about the  $x$  and  $y$  axes, the function  $\phi^1$  must define a representation under these transformations. One finds, just like in [15] that

$$\phi^1 \sim (-, +). \quad (3.5)$$

meaning that  $\phi^1$  is odd under  $(x, y) \rightarrow (-x, y)$  (the first sign) and even under  $(x, y) \rightarrow (x, -y)$  (the second sign). We can therefore choose to work with a fundamental domain  $Q_{2n}$  that is the part of the polygon on the first quadrant  $x, y \geq 0$ . The antisymmetry under  $x$  flips also implies that  $\phi^1$  vanishes on the part of the  $y$  axis inside the polygon:

$$\phi^1(x = 0, y) = 0. \quad (3.6)$$

Thus on the first quadrant,  $\phi^1$  vanishes on the  $y$  axis and on  $\tilde{e}_1$ . On the rest of the boundary the value of  $\phi^1$  must be left arbitrary. This completes the specification of  $\phi^1$  (see Figure 3).

Because of the rotation symmetry of the polygon, the calibrations  $u^\alpha$  and their associated exact parts  $d\phi^\alpha$ , with  $\alpha = 2, \dots, n$  are determined by  $u^1$  and  $\phi^1$ . Let  $(x_\alpha, y_\alpha)$  denote the points obtained by a counterclockwise rotation of  $(x, y)$  by an angle  $\theta_\alpha = \alpha \frac{\pi}{n}$ :

$$(x_{(\alpha)}, y_{(\alpha)}) = (x \cos \theta_\alpha - y \sin \theta_\alpha, x \sin \theta_\alpha + y \cos \theta_\alpha), \quad \theta_\alpha = \alpha \frac{\pi}{n}. \quad (3.7)$$

The various calibrations are mapped into each other by these rotations, thus we have

$$u^{\alpha+1}(x_{(\alpha)}, y_{(\alpha)}) = u^1(x, y). \quad (3.8)$$

More explicitly this gives

$$u^{\alpha+1}(x, y) = \cos \theta_\alpha dx + \sin \theta_\alpha dy + d\phi^1(x_{(-\alpha)}, y_{(-\alpha)}). \quad (3.9)$$

Comparing this result with the notation  $u^\alpha = \omega^\alpha + d\phi^\alpha$  we have

$$\omega^{\alpha+1} = \cos \theta_\alpha dx + \sin \theta_\alpha dy, \quad \text{and} \quad \phi^{\alpha+1}(x, y) = \phi^1(x_{(-\alpha)}, y_{(-\alpha)}). \quad (3.10)$$

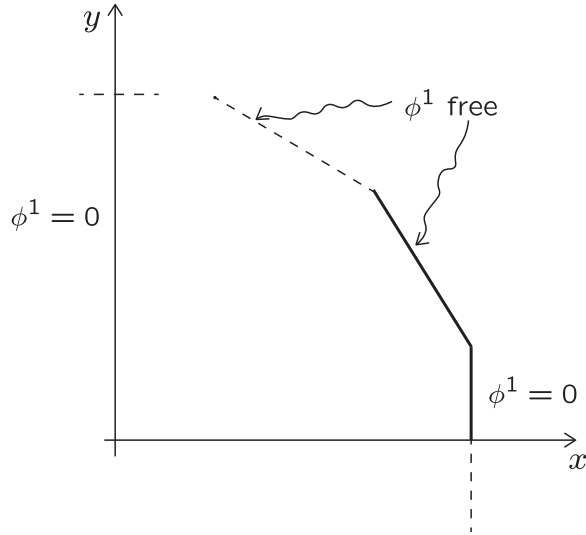


**Figure 3:** The part  $Q_{2n}$  of the polygon  $P_{2n}$  on the first quadrant is the fundamental domain for the function  $\phi^1$  entering the calibration  $u^1$ . The function  $\phi^1$  vanishes on the edge  $\bar{e}_1$  and on the  $y$  axis. There is no boundary condition for  $\phi^1$  over the other edges on the first quadrant.

If we know  $\phi^1$  over  $Q_{2n}$ , we know  $\phi^1$  everywhere, and therefore we know all the  $\phi^\alpha$  everywhere. The full set of calibrations is then known. Due to the choice of  $\omega^\alpha$  and the boundary conditions on  $\phi^\alpha$ , all calibrations  $u^\alpha$  satisfy the integral conditions on the curves in  $C_\alpha$ .

The program uses the fiducial norm squared of an arbitrary one form, given by:

$$|\alpha_x dx + \alpha_y dy|_0^2 \equiv \alpha_x^2 + \alpha_y^2. \quad (3.11)$$

The primal program then becomes

$$\begin{aligned} &\text{Minimize } \int_{P_{2n}} dx dy \Omega \quad \text{over } \Omega, \phi^\alpha, \quad \alpha = 1, \dots, n \\ &\text{subject to: } |u^\alpha|_0^2 - \Omega \leq 0, \quad \alpha = 1, \dots, n. \end{aligned} \quad (3.12)$$

Using the dihedral symmetry the objective can be written as

$$2 \cdot (2n) \int_{T_{2n}} dx dy \Omega, \quad (3.13)$$

and the optimization is carried out applying the constraints  $\Omega \geq |u^\alpha|_0^2$  over the region  $T_{2n}$ .

### 3.2 Dual Program

This time we need to determine functions  $\varphi^\alpha$  on the polygon  $P_{2n}$  with prescribed discontinuities  $\nu^\alpha$  across chosen curves  $m^\alpha \in C_\alpha$ . At the optimum the curves of constant  $\varphi^\alpha$  (in a region where  $\varphi^\alpha$  is not a constant) represent the saturating curves in the class  $C_\alpha$ .

Consider first the function  $\varphi^1$  associated with the class  $C_1$ . For this function we select the discontinuity to occur on the real  $x$  axis, along the curve  $x \in [-\frac{1}{2}, \frac{1}{2}], y = 0$ . We set

$$\varphi^1(x, 0^+) = \frac{1}{2}\nu, \quad \varphi^1(x, 0^-) = -\frac{1}{2}\nu, \quad (3.14)$$

This is a function with discontinuity  $\nu$ : The value of  $\varphi^1$  increases by  $\nu$  as  $y$  changes from  $0^-$  to  $0^+$ . The function  $\varphi^1$  transforms as a representation under the  $\mathbb{Z}_2 \times \mathbb{Z}_2$  group where the first factor refers to  $(x, y) \rightarrow (-x, y)$  and the second to  $(x, y) \rightarrow (x, -y)$ :

$$\varphi^1 \sim (+, -). \quad (3.15)$$

Consistent with the discontinuity,  $\varphi^1$  changes sign under  $y$  flips and is invariant under  $x$  flips. Note that when calculating  $\varphi^1$  derivatives in the program we do not include the contribution from the discontinuity. It follows from the above equation that  $Q_{2n}$  is a fundamental domain for  $\varphi^1$ . If known there, it is known all over the polygon.

Working over  $Q_{2n}$  we have the boundary condition  $\varphi^1 = \nu/2$  on the  $x$  axis. Over the edge  $\tilde{e}_1$  The function  $\varphi^1$  is free to vary over the edge  $\tilde{e}_1$  and over the  $y$  axis. Since no  $C_1$  geodesics can end on the other edges of the polygon and  $\varphi^1$  must be continuous except at the real axis,  $\varphi^1$  vanishes on all polygon edges on the first quadrant other than  $\tilde{e}_1$  (see Figure 4).

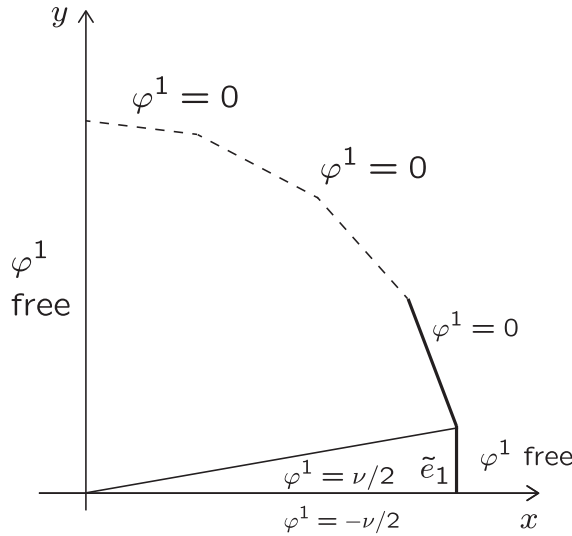


**Figure 4:** The part  $Q_{2n}$  of the polygon  $P_{2n}$  on the first quadrant is the fundamental domain for the function  $\varphi^1$ . The function is discontinuous by  $\nu$  across the  $x$  axis. It is free to vary over the edge  $\tilde{e}_1$  where the curves in  $C_1$  end, and on the  $y$  axis.  $\varphi^1$  vanishes on the other polygon edges on  $Q_{2n}$ .

As in (3.8), the other functions  $\varphi^\alpha$ ,  $\alpha = 2, \dots, n$ , are determined from  $\varphi^1$  via rotations:

$$\varphi^{\alpha+1}(x_{(\alpha)}, y_{(\alpha)}) = \varphi^1(x, y). \quad (3.16)$$

Using the transformations (3.15) of  $\varphi^1$  under reflections one can quickly write  $\varphi^\alpha$  on  $T_{2n}$ , for all  $\alpha = 2, \dots, n$  in terms of the values of  $\varphi^1$  on  $Q_{2n}$ . Since all the  $\varphi^\alpha$  are related to each other by rotations, the discontinuity parameters  $\nu^\alpha$  are all the same and equal to  $\nu$ .

An example, shown in Figure 5, applies to the evaluation of  $\varphi^2$  on  $T_{2n}$ . We have, by application of (3.16) for  $k = 1$ ,

$$\varphi^2(p) = \varphi^1(p'), \quad (3.17)$$

where  $p'$  is obtained from  $p$  by a clockwise rotation by  $\theta_1 = \pi/n$ . We also have, on account of (3.15),

$$\varphi^1(p') = -\varphi^1(p''), \quad (3.18)$$

where  $p''$  is the reflection of  $p'$  about the  $x$  axis. Therefore

$$\varphi^2(p) = -\varphi^1(p''), \quad (3.19)$$

expressing, as desired,  $\varphi^2$  on  $T_{2n}$  in terms of  $\varphi^1$  on  $Q_{2n}$ . Note, incidentally, that  $p$  and  $p''$  are related by reflection about the line joining the origin to the vertex at the top end of  $\tilde{e}_1$ .

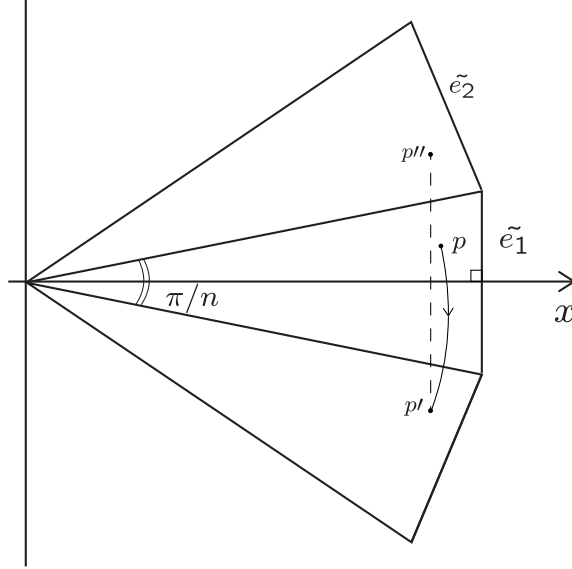


**Figure 5:** In order to write the dual program using the fundamental domain  $T_{2n}$  we need to evaluate all  $\varphi^\alpha$  on this domain. As illustrated here  $\varphi^2$  at  $p$  can ultimately be related to the value of  $\varphi^1$  at  $p''$ , the point obtained from  $p$  by a clockwise rotation by  $\pi/n$  followed by a reflection about the  $x$  axis.

The dual program as stated in [15], eqn.(2.7), takes the general form

$$\begin{aligned} \text{Maximize} \quad & 2 \sum_{\alpha} \nu^{\alpha} \ell_{\alpha} - \int_{M'} \omega_0 \left( \sum_{\alpha} |d\varphi^{\alpha}|_0 \right)^2 \quad \text{over } \nu^{\alpha} \text{ (constants), } \varphi^{\alpha} \text{ (functions)} \\ \text{subject to} \quad & \Delta\varphi^{\alpha}|_{m_{\alpha}} = -\nu^{\alpha}, \\ & \varphi^{\alpha}|_{\partial M} = 0, \quad \forall \alpha \in J. \end{aligned} \quad (3.20)$$

In our application  $\ell_{\alpha} = 1$  and  $\nu^{\alpha} = \nu$  for all  $n$  values of  $\alpha$ . Moreover,  $\omega_0 = dx \wedge dy$  and  $M'$  is the polygon  $P'_{2n}$  with the prime reminding us not to include the discontinuities in the evaluation of derivatives. While the above statement indicates that  $\varphi^{\alpha}$  is to vanish at the boundaries of the manifold, this requires some qualification: For the class  $C_{\alpha}$ , the edges  $e_{\alpha}, \tilde{e}_{\alpha}$  where the curves begin and end do not correspond to boundaries, and the values of  $\varphi^{\alpha}$  are unconstrained there. All other edges *are* boundaries and  $\varphi^{\alpha}$  must vanish on them. With these comments the program becomes:

$$\text{Maximize} \quad 2n\nu - \int_{P'_{2n}} dx dy \left( \sum_{\alpha} |d\varphi^{\alpha}|_0 \right)^2 \quad \text{over } \nu \text{ (constant), } \varphi^1 \text{ (function)} \quad (3.21)$$

Under the symmetry conditions that we impose, the integral over  $P'_{2n}$  is equal to  $4n$  times the integral over  $T_{2n}$ :

$$\int_{P'_{2n}} dx dy \left( \sum_{\alpha} |d\varphi^{\alpha}|_0 \right)^2 = 4n \int_{T_{2n}} dx dy \left( \sum_{\alpha} |d\varphi^{\alpha}|_0 \right)^2. \quad (3.22)$$

As discussed above, this integral can be evaluated if we know  $\varphi^1$  over  $Q_{2n}$ . Thus  $\nu$  and  $\varphi^1$  over  $Q_{2n}$  (with its boundary conditions), are the maximization variables.

As shown in [14] in the general dual problem the extremal area  $A$  and the extremal value of the  $\nu^\alpha$  are related as  $A = \sum_\alpha \nu^\alpha \ell_\alpha$ . For our case, with all  $\nu$ 's identical and  $\ell_s = 1$  this gives for the polygon  $P_{2n}$  an extremal area  $A_{2n}$  of value

$$A_{2n} = n\nu. \quad (3.23)$$

### 3.3 Edge length and height parameter

In this section we show that the edge length  $L_e$  of the polygon on the extremal metric is also related to the value of the  $\nu$  parameter. In this way  $L_e$  is also related to the extremal area.

We consider a vertex of the polygon  $P_{2n}$ . As we will discuss further later, for each vertex of the polygon there exists a region containing the vertex and half of the edges emerging from that vertex in which there are exactly two bands of systolic geodesics. As established in [13] the two bands are orthogonal and the metric is flat in this region. This situation is illustrated in Figure 6. There we show edges  $e_1$  and  $e_2$  attached to a vertex  $Q$  and the geodesics that end of them. The figures uses the conformal frame in which the angle at the vertex  $Q$  is  $\frac{\pi}{2}$ , rather than the original frame where the angle is the internal angle of the polygon at a vertex. Point  $P$  is the midpoint of  $e_1$  and point  $R$  is the midpoint of  $e_2$ . The line  $PO$  is the central geodesic of the first band, the band that ends on  $e_1$ , while the line  $RO$  is the central geodesic of the second band, the band that ends on  $e_2$ . The region bounded by the curved line from  $P$  to  $R$  and the edges  $e_1$  and  $e_2$  is the region with two bands of geodesics. The curve  $PR$  is the boundary geodesic of another band and above this curve we have a region with three or more bands of geodesics. It is crucial for the argument below that the edge lines  $PQ$  and  $QR$  are boundaries of a two-band region. Thus the boundary geodesic  $PR$  runs from one edge midpoint to the next. This was assumed but not proven in [13] and is not proven here either.

As discussed in [14] we can construct Gaussian coordinate systems adapted to a given set of systolic geodesics. We have coordinates  $(x^1, \varphi^1)$  associated with the systolic geodesics that end on  $e_1$  and  $(x^2, \varphi^2)$  associated with the systolic geodesics that end on  $e_2$ . The extremal metric in this common region can be written in two equivalent forms

$$\begin{aligned} ds^2 &= (dx^1)^2 + \frac{1}{(h_1)^2} (d\varphi^1)^2, \\ ds^2 &= (dx^2)^2 + \frac{1}{(h_2)^2} (d\varphi^1)^2. \end{aligned} \quad (3.24)$$

Clearly,  $x^1$  parameterizes by length the geodesics that end on  $e_1$  and  $x^2$  parameterizes by length the geodesics that end on  $e_2$ . Since the geodesics have length one, and we define the range of  $x^1$  and  $x^2$  symmetrically, the edge  $e_1$  is a line with  $x^1 = 1/2$  and the edge  $e_2$  is a line with  $x^2 = 1/2$ . Here  $h_1(x^1, \varphi^1)$  and  $h_2(x^2, \varphi^2)$  are two functions that quantify the density of systolic geodesics. Moreover, as was also proven in [14], over the region where only two bands exist, these functions satisfy

$$|h_1| + |h_2| = 1. \quad (3.25)$$

We will now show that these functions are in fact constants over the two band region. For this purpose a coordinate system defined by  $x^1$  and  $x^2$  above is useful. Recalling that  $|dx^1| = |dx^2| = 1$

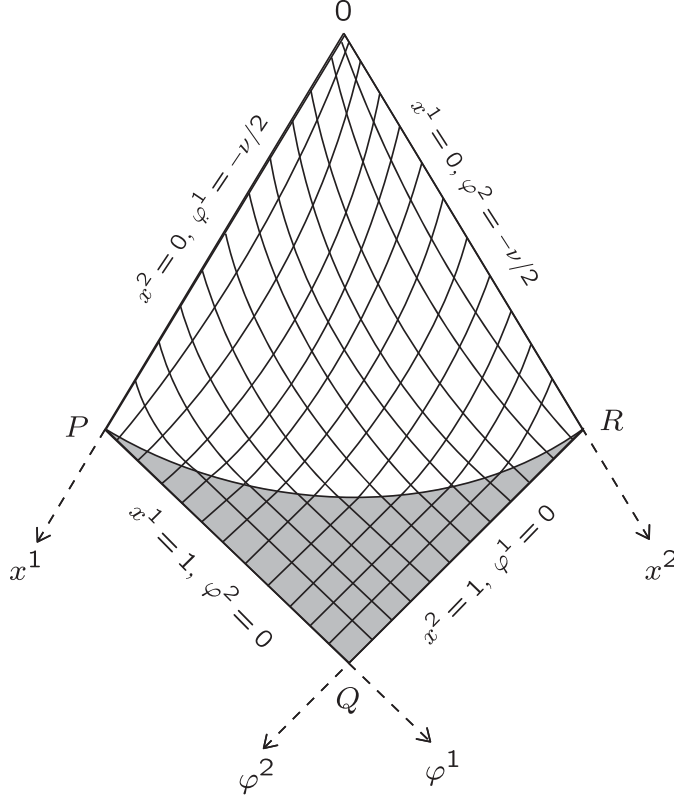


**Figure 6:** In the regions of the polygon where there are exactly two bands of systolic geodesics the bands are orthogonal. The curves ending on the edge  $e_1$  (the PQ segment) belong to the first band. They are parameterized by  $x^1$ , and are curves of constant  $\varphi^1$ . The curves ending on the edge  $e_2$  (the QR segment) belong to the second band. They are parameterized by  $x^2$ , and are curves of constant  $\varphi^2$ . Indicated are also the geodesics with  $\varphi^1 = -\nu/2$  and with  $\varphi^2 = -\nu/2$ , with endpoints the midpoints of hexagon edges.

the inverse metric takes the form

$$g^{-1} = \begin{pmatrix} 1 & f \\ f & 1 \end{pmatrix}, \quad f = \langle dx^1, dx^2 \rangle = \langle \hat{u}^1, \hat{u}^2 \rangle. \quad (3.26)$$

Here  $\hat{u}^i$  is the vector associated with the one form  $u_i$  and it is tangent to the geodesics in the  $i$ -th band. Since the geodesics are orthogonal  $f = 0$  and the metric simplifies tremendously:

$$ds^2 = (dx^1)^2 + (dx^2)^2. \quad (3.27)$$

We now exploit the compatibility of the three forms of the metric. Consider the function  $\varphi^1(x^1, x^2)$  expressing the coordinate  $\varphi^1$  in terms of the values of the coordinates  $x^1$  and  $x^2$ . Then back on the first metric in (3.24) and comparing with (3.27) we have

$$(dx^1)^2 + \frac{1}{(h_1)^2} (\partial_1 \varphi^1 dx^1 + \partial_2 \varphi^1 dx^2)^2 = (dx^1)^2 + (dx^2)^2. \quad (3.28)$$

Two conditions follow:

$$\partial_1 \varphi^1 = 0, \quad \partial_2 \varphi^1 = \pm h_1. \quad (3.29)$$

Using the second form for the metric in (3.24), analogous conditions are obtained for  $\varphi^2$ :

$$\partial_2\varphi^2 = 0, \quad \partial_1\varphi^2 = \pm h_2. \quad (3.30)$$

The first set of equations tells us that  $\varphi^1$  is just  $\varphi^1(x^2)$ , with no  $x^1$  dependence. It also tells us that

$$\frac{d\varphi^1}{dx^2}(x^2) = \pm h_1(x^1, \varphi^1(x^2)). \quad (3.31)$$

Similarly  $\varphi^2$  is just  $\varphi^2(x^1)$ , and

$$\frac{d\varphi^2}{dx^1}(x^1) = \pm h_2(x^2, \varphi^2(x^1)). \quad (3.32)$$

In (3.31) the left-hand side does not depend on  $x^1$  and in (3.32) the left-hand side does not depend on  $x^2$ . The same must hold for the right-hand sides and therefore  $h_1 = \tilde{h}_1(x^2)$ , is just a function of  $x^2$  and  $h_2 = \tilde{h}_2(x^1)$ . But then the condition (3.25) gives

$$|\tilde{h}_1(x^2)| + |\tilde{h}_2(x^1)| = 1. \quad (3.33)$$

Since  $x^1$  and  $x^2$  can be varied independently, the only possible solution is that both functions are constants. We have thus learned that both  $|h_1|$  and  $|h_2|$  are constants that add up to 1.

Note now that the geodesics with  $\varphi^1 = -\nu/2$  and  $\varphi^2 = -\nu/2$  hit the polygon boundary at the middle of the edges, points  $P$  and  $R$ , respectively; this is simply the way we defined the functions  $\varphi$ . Let  $L_e$  denote the length of the edges in the extremal metric. Because of the symmetry of this metric the half-length  $\frac{1}{2}L_e$  is both the distance from  $P$ , where  $\varphi^1 = -\nu/2$ , to the vertex  $Q$ , where  $\varphi^1 = 0$ , as well as the distance from  $R$ , where  $\varphi^2 = -\nu/2$ , to the vertex  $Q$ , where  $\varphi^2 = 0$ . For the first,  $x^1$  is constant, and for the second  $x^2$  is constant. We thus have, integrating the length element over these intervals:

$$\begin{aligned} \frac{1}{2}L_e &= \int_{-\nu/2}^0 \frac{d\varphi^1}{|h_1|} = \frac{\nu}{2|h_1|}, \\ \frac{1}{2}L_e &= \int_{-\nu/2}^0 \frac{d\varphi^2}{|h_2|} = \frac{\nu}{2|h_2|}. \end{aligned} \quad (3.34)$$

This implies  $|h_1| = |h_2| = \frac{1}{2}$ . As a result,

$$L_e = 2\nu. \quad (3.35)$$

This is what we wanted to show and holds for all  $2n$ -gons.

Given the above result for the edge length  $L_e$ , the perimeter  $\mathcal{P}_{2n}$  of the polygon is given by  $\mathcal{P}_{2n} = 2nL_e = 4n\nu$ . Recalling from (3.23) that the extremal area is  $A_{2n} = n\nu$  we find the perimeter/area relation:

$$A_{2n} = \frac{1}{4}\mathcal{P}_{2n}, \quad \ell_s = 1. \quad (3.36)$$

This is for the value  $\ell_s = 1$  of the systole. If we introduce an arbitrary systole  $\ell_s$  back into this formula by scaling of the extremal metric we

$$A_{2n} = \frac{1}{4}\ell_s\mathcal{P}_{2n}. \quad (3.37)$$



This formula is as if the surface was built (which is not) by piling flat little triangles of height  $\ell_s/2$  all over the length of the perimeter. In fact for the flat metric  $\rho = 1$  on a regular  $2n$ -sided polygon, one quickly notes that the area  $\bar{A}_{2n}$  and the perimeter  $\bar{\mathcal{P}}_{2n}$  are related by

$$\bar{A}_{2n} = \frac{1}{2} \cdot a \cdot \bar{\mathcal{P}}_{2n}, \quad (3.38)$$

where  $a$  is the apothem. Since we take  $a = \frac{1}{2}$  in our canonical presentation we have

$$\bar{A}_{2n} = \frac{1}{4} \bar{\mathcal{P}}_{2n}, \quad a = \frac{1}{2}, \quad (3.39)$$

the same relation that holds for the extremal metric with  $\ell_s = 1$ . It follows that with  $\ell_s = 1$  and apothem  $\frac{1}{2}$ :

$$\frac{\mathcal{P}_{2n}}{\bar{\mathcal{P}}_{2n}} = \frac{A_{2n}}{\bar{A}_{2n}} < 1. \quad (3.40)$$

In passing from the flat metric to the extremal metric, the fractional reduction in area equals the fractional reduction of the perimeter, or the fractional reduction of the edge length.

## 4 Calabi's hexagon

In this section we discuss the extremal problem for Calabi's hexagon  $P_6$ . We give the setup of the primal and the dual programs in detail. We then present our numerical solution, which gives quantitative support for the qualitative picture provided by Calabi. We also discuss the distribution of curvature on the surface showing there is positive curvature on the three-band region and line curvature on the boundary of this region.

### 4.1 Setup for convex programs

Here we formulate the primal and the dual programs for the hexagon explicitly. We will follow the general theory developed in sections 3.1 and 3.2 and specialize to  $n = 3$ . From eqs. (3.1) and (3.10) the three calibrations can be written as

$$\begin{aligned} u^1 &= dx + d\phi^1, \\ u^2 &= \frac{1}{2}dx + \frac{\sqrt{3}}{2}dy + d\phi^2, \\ u^3 &= -\frac{1}{2}dx + \frac{\sqrt{3}}{2}dy + d\phi^3. \end{aligned} \quad (4.1)$$

Due to the hexagonal symmetry we only need to compute the minimal area metric on  $T_6$ . For the primal program we need the three functions  $\phi^1, \phi^2$  and  $\phi^3$  on  $T_6$ . Using the symmetries of the hexagon one can define  $\phi^2$  and  $\phi^3$  in terms of  $\phi^1$  if we know the value of  $\phi^1$  over  $Q_6$ , the part of  $P_6$  in the first quadrant. We can explain this clearly using Figure 7. The value of  $\phi^2$  at a point  $P \in T_6$  is equal to the value of  $\phi^1$  at the point  $P_{-1}$ , which is same as the value of  $\phi^1$  at the point  $P_{-1,x} \in Q_6$ . This lets us determine  $\phi^2$  everywhere on  $T_6$  with the formula:

$$\phi^2(x, y) = \phi^1\left(\frac{1}{2}x + \frac{\sqrt{3}}{2}y, \frac{\sqrt{3}}{2}x - \frac{1}{2}y\right). \quad (4.2)$$

In a similar fashion, the value of  $\phi^3$  at point  $P \in T_6$  is equal to the value of  $\phi^1$  at the point  $P_{-2}$ . This is same as the value of  $\phi^1$  at the point  $P_{-2,x}$  which is negative of the value of  $\phi^1$  at the point  $P_{-2,x,y} \in Q_6$ . This lets us determine  $\phi^3$  over  $T_6$  in terms of  $\phi^1$  over  $Q_6$ :

$$\phi^3(x, y) = -\phi^1\left(\frac{1}{2}x - \frac{\sqrt{3}}{2}y, \frac{\sqrt{3}}{2}x + \frac{1}{2}y\right). \quad (4.3)$$

The boundary conditions for  $\phi^1$  on  $Q_6$  are those described in Figure 3:  $\phi^1$  is zero on  $\tilde{e}_1$  and on the

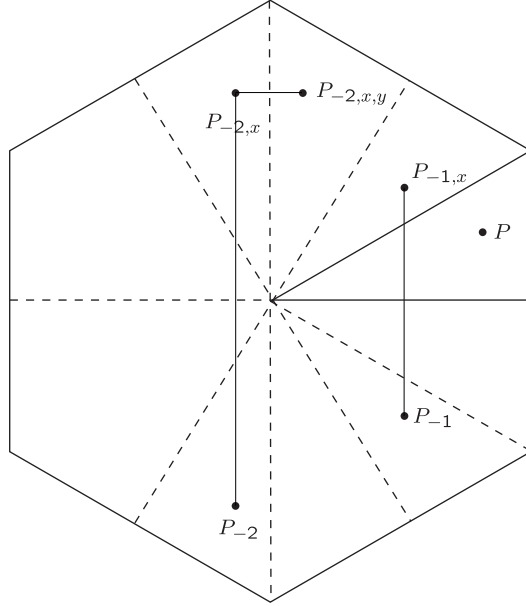


**Figure 7:** The values of  $\phi^2$  and  $\phi^3$  over  $T_6$  are related to values of  $\phi^1$  over  $Q_6$ . The point  $P_{-1}$  is a rotation of  $P \in T_6$  by  $-\frac{\pi}{3}$ .  $P_{-1,x} \in Q_6$  is the reflection of  $P_{-1}$  about the  $x$ -axis. The point  $P_{-2}$  is a rotation of  $P$  by  $-\frac{2\pi}{3}$ .  $P_{-2,x}$  is the reflection of  $P_{-2}$  about the  $x$ -axis.  $P_{-2,x,y} \in Q_6$  is the reflection of  $P_{-2,x}$  about the  $y$ -axis.

$y$  axis, and it is free on the other edges on  $Q_6$ . The program is then explicitly defined by

$$\begin{aligned} & \text{Minimize } 12 \int_{T_6} dx dy \Omega \quad \text{over } \Omega \text{ and } \phi^1, \\ & \text{subject to: } |u^i|_0^2 - \Omega \leq 0, \quad i = 1, 2, 3. \end{aligned} \tag{4.4}$$

The fiducial norms of the one-forms are given by

$$\begin{aligned} |u^1|_0^2 &= (1 + \partial_x \phi^1)^2 + (\partial_y \phi^1)^2, \\ |u^2|_0^2 &= \left(\frac{1}{2} + \partial_x \phi^2\right)^2 + \left(\frac{\sqrt{3}}{2} + \partial_y \phi^2\right)^2, \\ |u^3|_0^2 &= \left(-\frac{1}{2} + \partial_x \phi^3\right)^2 + \left(\frac{\sqrt{3}}{2} + \partial_y \phi^3\right)^2. \end{aligned} \tag{4.5}$$

We now give the explicit setup for the dual program. Having three homology classes of curves we need to define three functions  $\varphi^1, \varphi^2$ , and  $\varphi^3$  over  $P_6$ . Each function must have a discontinuity across some arbitrarily selected curve in the corresponding class. We choose  $\varphi^1$  to be discontinuous across the  $x$ -axis:

$$\varphi^1(x, 0^-) = -\frac{\nu}{2} \quad \text{and} \quad \varphi^1(x, 0^+) = \frac{\nu}{2}. \tag{4.6}$$

The function  $\varphi^1$  is free to vary on the edge  $\tilde{e}_1$  and on the  $y$  axis and vanishes on the other edges in  $Q_6$  (as was summarized in Figure 4). The hexagonal symmetry can then be used to determine

$\varphi^2, \varphi^3$  in terms of  $\varphi^1$  as we did in the case of the primal program. This time, however,  $\varphi^1$  is odd under reflections about the  $x$  axis and even under reflections about the  $y$  axis. This gives,

$$\begin{aligned}\varphi^2(x, y) &= -\varphi^1\left(\frac{1}{2}x + \frac{\sqrt{3}}{2}y, \frac{\sqrt{3}}{2}x - \frac{1}{2}y\right), \\ \varphi^3(x, y) &= -\varphi^1\left(\frac{1}{2}x - \frac{\sqrt{3}}{2}y, \frac{\sqrt{3}}{2}x + \frac{1}{2}y\right).\end{aligned}\tag{4.7}$$

The dual program is then explicitly written as

$$\text{Maximize } 6\nu - 12 \int_{T_6} dx dy \left( |d\varphi^1|_0 + |d\varphi^2|_0 + |d\varphi^3|_0 \right)^2 \text{ over } \nu \text{ and } \varphi^1.\tag{4.8}$$

A numerical solution of the program requires discretization (see appendix A).

## 4.2 Numerical results, metric description, and consistency checks

We now present our results from the numerical evaluation of the primal and the dual programs for the hexagon. From the solution of the dual program one can construct the saturating geodesics in classes  $C_1, C_2$ , and  $C_3$  as curves of constant  $\varphi^1, \varphi^2$ , and  $\varphi^3$ , respectively. Doing so results in the picture of  $P_6$  shown in Figure 8. There are regions  $U_3$  and  $U_2$  with three and two bands of geodesics, respectively. The central region of the hexagon defines the whole of  $U_3$ . Finite neighborhoods of each vertex are in  $U_2$ . There are no regions  $U_1$  or  $U_0$ . The boundary of the region  $U_3$  touches the edges of the polygon at the midpoints. It is also clear from the figure and the data that, as expected, the geodesics in  $U_2$  intersect at right angles – a property proven in [13]. This means that at the vertices of the polygon we have effectively an internal angle of  $\pi/2$ , rather than the apparent  $2\pi/3$ . The extremal conformal metric in fact diverges as we approach the vertices, and the conformal map turning the angle from  $2\pi/3$  to  $\pi/2$  renders the metric finite.

Each band of geodesics is defined by a pair of opposite edges  $e_i$  and  $\tilde{e}_i$ , and each edge determines two vertices at its endpoints. Each band has two *boundary* geodesics, each departing from a vertex in  $e_i$  and ending on a vertex in  $\tilde{e}_i$ . As conjectured in [13], each boundary geodesic follows the (neighboring) edge until the midpoint before veering off into the inside of the polygon. It is clear it cannot veer off before reaching the midpoint, as then we would have a region near the midpoint of each edge with just one band of geodesics, which is impossible in a Riemannian isosystolic problem. If it were to veer off after the midpoint there is no obvious contradiction, but the situation would be less symmetric, with  $U_3$  overlapping with the edges over finite regions. In section 3.3 we showed that the edge length  $L_e$  is equal to  $2\nu$  using the assumption that boundary geodesics veer off at midpoints. We will see that the data below gives evidence for this relation.

A few more observations follow from the use of the Gauss-Bonnet formula giving the Euler number  $\chi$  of a surface with a boundary

$$\chi = \frac{1}{2\pi} \int K dA + \frac{1}{2\pi} \int k ds + \frac{1}{2\pi} \sum_i (\pi - \theta_i),\tag{4.9}$$

Here  $K$  is the Gaussian curvature,  $k$  is the curvature on the boundary, which vanishes when the boundary is a geodesic, and  $\theta_i \in (0, 2\pi)$  is the internal angle at corners that appear on the boundary. Since  $U_3$  is topologically a disk it has  $\chi = 1$ . The boundary of  $U_3$  is a connected curve comprised of

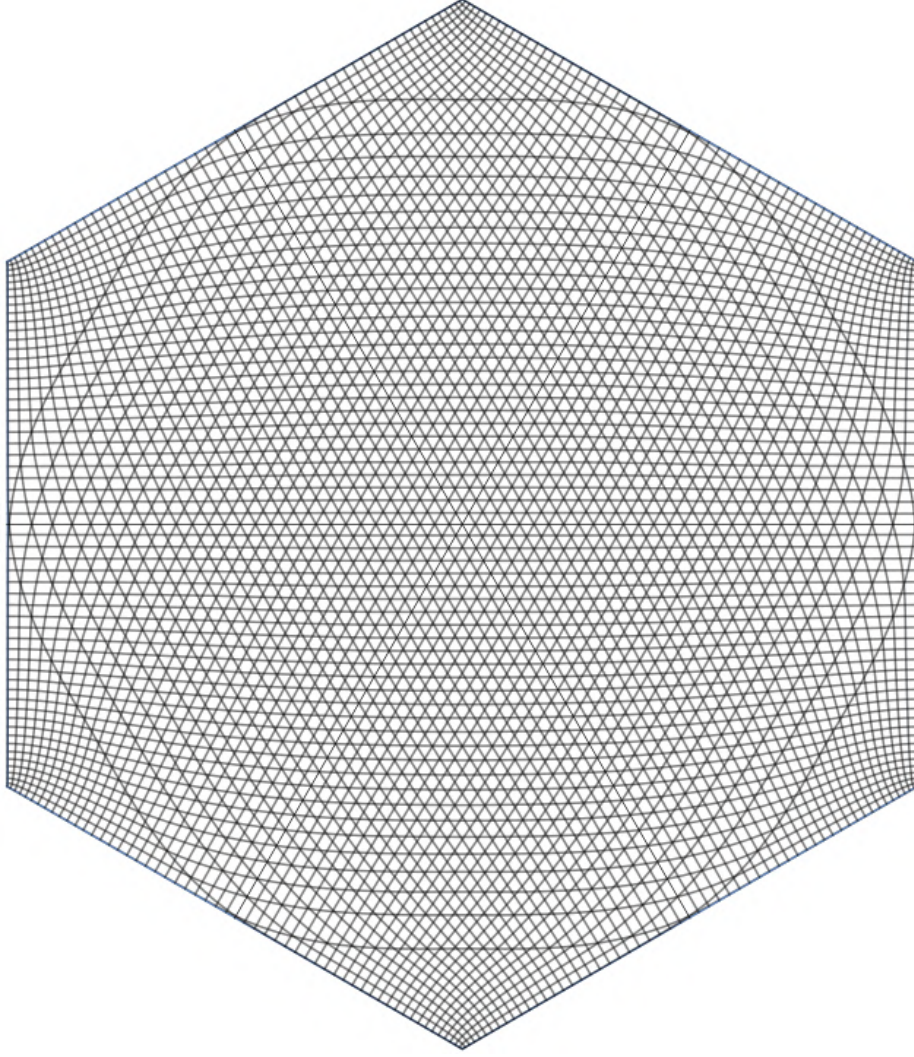


**Figure 8:** Saturating geodesic curves in the minimal area metric for Calabi’s hexagon. The surface is covered by a connected region  $U_3$  with three geodesic bands and six regions comprising the two-band part  $U_2$ , each region around a vertex. The metric is flat on  $U_2$  but has Gaussian curvature on  $U_3$  and line curvature supported on the boundary of  $U_3$ .

boundary geodesics that join at edge midpoints without forming corners. It follows that the second and third contributions in the Gauss-Bonnet formula vanish and

$$\frac{1}{2\pi} \int_{U_3} K dA = 1. \tag{4.10}$$

Now consider applying Gauss-Bonnet to the whole surface, which is still a topological disk. The internal angle at each of the six corners is  $\theta_i = \frac{\pi}{2}$ . Moreover  $\partial U_3$  has six arcs, each going from the midpoint of an edge to the midpoint of the next edge. These arcs are geodesics on  $U_3$  but are not geodesics on  $U_2$ . As a result they carry line curvature singularity on the surface. The amount of curvature in each arc is computed from the turning angle of the tangent vector to the arc as seen from the flat metric in  $U_2$ . The turning angle is in fact  $\frac{\pi}{2}$  (a fourth of  $2\pi$ ) but as a  $U_2$  boundary the

sign of  $k$  is negative. We thus have, for each arc and for each corner:

$$\frac{1}{2\pi} \int_{\text{arc}} k ds = -\frac{1}{4}, \quad \frac{1}{2\pi} (\pi - \theta_i) = +\frac{1}{4}. \quad (4.11)$$

Since we have six arcs and six corners the contributions to the Euler number of the whole surface cancel:

$$\chi = 1 + 6(-\frac{1}{4}) + 6(\frac{1}{4}) = 1. \quad (4.12)$$

It is also possible to check that over each band  $\mathcal{B}$  of geodesics the total integrated curvature vanishes:

$$\int_{\mathcal{B}} K dA + \int k ds = 0. \quad (4.13)$$

This must happen because we can glue the beginning and ending edges of the band to form an annulus, a surface with  $\chi = 0$ . This is simple to confirm. Since any band in the hexagon contains the full  $U_3$  the bulk contribution above is  $2\pi$ . The integral  $\int k ds$  represents the contribution of line curvature in the annulus. There is no contribution from the boundary of the band since those are geodesics in the band. But each band contains in its interior four arcs with line curvature, the arcs on the four vertices that define the band. We saw that each one contributes  $-\frac{\pi}{2}$  to  $\int k ds$ , and therefore this gives a total of  $-2\pi$  canceling the bulk contribution, as expected.

Before looking at the numerical results it is useful to consider the reference flat metric  $\rho = 1$ , which is admissible. The area  $\bar{A}_6$  of the hexagon in this metric is

$$\bar{A}_6 = \frac{\sqrt{3}}{2} \simeq 0.866025. \quad (4.14)$$

The perimeter  $\bar{\mathcal{P}}_6$  of the polygon in this metric is

$$\bar{\mathcal{P}}_6 = 2\sqrt{3} \simeq 3.464102. \quad (4.15)$$

Note the exact relation  $\bar{\mathcal{P}}_6 = 4\bar{A}_6$  anticipated in (3.39). Recall also the dual program prediction (3.36):  $\mathcal{P}_6 = 4A_6$ , valid for the extremal metric.

We have below data for various quantities computed with the primal and with the dual programs at various values of the lattice resolution  $N_c$  (essentially the number of subdivisions of the apothem, see Appendix A for more details). To get some additional information from the data, we analyze convergence and try extrapolation to  $N_c \rightarrow \infty$  in the same manner as done in [15]. From the data for  $N_c = 2, 4, \dots, 128$  we define the error  $e_q(N_c)$  in a quantity  $q$  at resolution  $N_c$  by

$$e_q(N_c) \equiv q(N_c) - q(128), \quad N_c = 2, 4, \dots, 64. \quad (4.16)$$

We then fit  $e_q(N_c)$  to a decaying exponential function,

$$e_q(N_c) = \frac{a}{N_c^b}, \quad (4.17)$$

to find the values of  $a$  and  $b$ , with  $b$  giving information on the convergence rate. The extrapolated value  $q_*$  of  $q$  at infinite resolution is estimated by

$$q_* = q(128) - e_q(128). \quad (4.18)$$

Table 1 contains the data for the area  $A_6$ , perimeter  $\mathcal{P}_6$ , and metric  $\rho^2 = \Omega$  at the origin, as computed from the primal program at various values of  $N_c$ , including the  $N_c \rightarrow \infty$  extrapolation.

The area goes monotonically down, as it should upon minimization with lattices that fit evenly into each other. The perimeter is evaluated by integrating the metric along the edges. This is difficult to do accurately, since the discretized metric tries to diverge as we approach the vertices of the hexagon. The convergence of the perimeter data is certainly not monotonic. Nor is the convergence monotonic for the metric at the center of the hexagon.

The data from the dual program is presented in table 2. The dual program directly solves for the minimal area and the value of  $\nu$ . It also gives us the functions  $\varphi^\alpha$ ,  $\alpha = 1, 2, 3$ , from which we compute the metric  $\rho = \sum_\alpha |d\varphi^\alpha|_0$ . The table shows the value of the area  $A_6$ , the perimeter  $\mathcal{P}_6$ , the metric  $\rho^2 = \Omega$  at the origin, and  $2\nu$ .

Let us look first at the area. Based on the bounds obtained by the  $N_c = 128$  data of the two programs we find that the extremal area of the hexagon is in the range

$$0.8400 < A_6 < 0.8414. \quad (4.19)$$

The error analysis shows that convergence is slow for the primal but faster in the dual ( $b \sim 0.9$  and  $b = 1.6$ , respectively). The dual extrapolation suggests that the value  $A_6 = 0.8401$  could be correct to four significant digits. This area, in fact, is only 3% lower than the flat-metric area  $\bar{A}_6 = \frac{\sqrt{3}}{2}$ .

The perimeter  $\mathcal{P}_6$  can be used to test the expected relation  $\mathcal{P}_6 = 4A_6$  which, as explained before, is derived rigorously once we assume that boundary geodesics veer off at edge midpoints. The equation holds to great accuracy for  $N_c = 128$  in the dual program ( $3.3647/0.84002 = 4.0055$ ). It holds less accurately in the primal at the same resolution ( $3.3275/0.84135 = 3.95495$ ), a 1% error. The value of the metric at the origin in both the primal and dual programs seem consistent with each other. Finally the relation  $A_6 = 3\nu$ , that follows from the dual program, is seen to hold very accurately.

$N_c$	$A_6$	$\mathcal{P}_6$	$\rho^2(0,0)$
2	0.86602	3.4641	1.00000
4	0.86297	3.3888	1.04921
8	0.85389	3.2774	1.14853
16	0.84819	3.2746	1.17448
32	0.84458	3.2894	1.17072
64	0.84249	3.3092	1.16571
128	0.84135	3.3275	1.16060
$\rightarrow \infty$	0.84028	3.3275	1.16167

**Table 1:** Primal program numerical data for the hexagon area  $A_6$ , perimeter  $\mathcal{P}_6$ , and metric  $\rho^2(0,0)$  at the origin at various choices of lattice resolution  $N_c$ .

## 5 The cases of the octagon and decagon

In this section we discuss in some detail the octagon and then, more briefly, the decagon. There are a few reasons to do this explicitly. There are no known extremal metrics with regions covered by a finite number  $k$  of geodesic bands with  $k > 3$ . Thus the octagon and decagon provide, respectively, tractable examples with regions having four and five bands of geodesics. The octagon has regions

$N_c$	$A_6$	$\mathcal{P}_6$	$\rho^2(0,0)$	$2\nu$
2	0.80535	2.9554	1.15614	0.5369
4	0.82766	2.9627	1.17678	0.5518
8	0.83581	3.0499	1.15032	0.5571
16	0.83866	3.1755	1.15557	0.5592
32	0.83964	3.2944	1.15295	0.5598
64	0.83997	3.3873	1.15659	0.5599
128	0.84002	3.3647	1.15680	0.5597
$\rightarrow \infty$	0.84007	3.4251	1.15656	0.5598

**Table 2:** Dual program numerical data for the hexagon area  $A_6$ , perimeter  $\mathcal{P}_6$ , metric  $\rho^2(0,0)$  at the origin, and  $2\nu$  at various choices of lattice resolution  $N_c$ .

$U_4$ ,  $U_3$ , and  $U_2$ . The possibility has been raised [17] that in the isosystolic problem any  $U_4$  could be forced to have zero Gaussian curvature, but our results indicate that the integrated curvature on  $U_4$  should be that of half a sphere. (We are not able to assess the curvature on the region  $U_3$ .) We will also see that the region  $U_4$  is rather large, while  $U_3$  and  $U_2$  are small. It was stated in [17] that in the isosystolic problem any  $U_5$  must have zero Gaussian curvature. Our results for the decagon, however, indicate that the integrated curvature on  $U_5$  should be that of half a sphere.

## 5.1 Setup for the convex programs

For the primal program the four calibrations are given by:

$$\begin{aligned}
u^1 &= dx + d\phi^1, \\
u^2 &= \frac{1}{\sqrt{2}}dx + \frac{1}{\sqrt{2}}dy + d\phi^2, \\
u^3 &= dy + d\phi^3, \\
u^4 &= -\frac{1}{\sqrt{2}}dx + \frac{1}{\sqrt{2}}dy + d\phi^4.
\end{aligned} \tag{5.1}$$

We need the four functions  $\phi^1, \phi^2, \phi^3$ , and  $\phi^4$  on  $T_8$ . Due to the symmetries of the octagon we can define all functions on  $T_8$  in terms of just  $\phi^1$  on  $Q_8$ , the piece of the octagon on the first quadrant. The precise relations are:

$$\begin{aligned}
\phi^2(x, y) &= \phi^1\left(\frac{x+y}{\sqrt{2}}, \frac{x-y}{\sqrt{2}}\right), \\
\phi^3(x, y) &= \phi^1(y, x), \\
\phi^4(x, y) &= -\phi^1\left(\frac{x-y}{\sqrt{2}}, \frac{x+y}{\sqrt{2}}\right).
\end{aligned} \tag{5.2}$$

The boundary conditions for  $\phi^1$  on  $Q_8$  are those described in Figure 3:  $\phi^1$  is zero on  $\tilde{e}_1$  and on the  $y$  axis, and it is free on the other edges on  $Q_8$ . The primal program for the octagon is then:

$$\begin{aligned}
&\text{Minimize } 16 \int_{T_8} dx dy \Omega \quad \text{over } \Omega \quad \text{and } \phi^1, \\
&\text{subject to: } |u^i|_0^2 - \Omega \leq 0, \quad i = 1, 2, 3, 4.
\end{aligned} \tag{5.3}$$

For the dual program, the functions  $\varphi^2$ ,  $\varphi^3$  and  $\varphi^4$  are related to  $\varphi^1$  as follows:

$$\begin{aligned}\varphi^2(x, y) &= -\varphi^1\left(\frac{x+y}{\sqrt{2}}, \frac{x-y}{\sqrt{2}}\right), \\ \varphi^3(x, y) &= -\varphi^1(y, x), \\ \varphi^4(x, y) &= -\varphi^1\left(\frac{x-y}{\sqrt{2}}, \frac{x+y}{\sqrt{2}}\right).\end{aligned}\tag{5.4}$$

On  $Q_8$  the boundary conditions on  $\varphi^1$  are: it is equal to  $\nu/2$  on the  $x$  axis, it free to vary on the edge  $\tilde{e}_1$  and on the  $y$  axis, and vanishes on the other octagon edges of  $Q_8$ . The dual program is then explicitly written as:

$$\text{Maximize } 8\nu - 16 \int_{T_8} dx dy \left( |d\varphi^1|_0 + |d\varphi^2|_0 + |d\varphi^3|_0 + |d\varphi^4| \right)^2 \text{ over } \nu \text{ and } \varphi^1.\tag{5.5}$$

The discretization scheme we use for the octagon is different from that of the hexagon and admits a simple generalization to  $2n$ -gons (see Appendix A).

## 5.2 Numerical results and patterns of bands

Now we present the results from the primal and the dual program for the octagon. The picture of saturating geodesics on  $P_8$  which is constructed from our solution is given in Figure 9.

The central region is covered by four geodesic bands and has positive curvature. There is a small region with three geodesics near each of the edges. The regions with two geodesics are flat. These regions are easier to see in Figure 10 where we draw the boundary geodesics in classes  $C_1, C_2, C_3$ , and  $C_4$ .

The best result for the area in the primal program, giving an upper bound, was obtained with  $N_c = 128$ . For the dual program, giving us a lower bound, we could only work up to  $N_c = 64$ . Together they give

$$0.7776 < A_8 < 0.7804.\tag{5.6}$$

As in the case of the hexagon, the convergence is faster in the dual program, and extrapolation suggests that  $A_8 = 0.778$  could be correct to three significant digits. The flat metric area of the octagon is  $\bar{A}_8 = 2 \tan(\pi/8) \simeq 0.82843$ . This means that the extremal area is about 6.1% lower than the area of the flat-metric. This is a larger decrease compared to the case of the hexagon. For the perimeter, we find that the relation  $\mathcal{P}_8 = 4A_8$  holds in the dual program with an accuracy of 3%. Finally the relation  $A_8 = 4\nu$  holds very accurately.

Let us now consider curvature. For this we can first consider the region  $U_4$  which is topologically a disk. To figure out the extent of the various  $U_k$  on the surface one must draw all boundary geodesics for the four bands (a total of 8). The boundary of  $U_8$  is given by eight geodesic arcs. Each arc corresponds to a different boundary geodesic. Figure 10 makes it very plausible that the arcs join smoothly without corners. That being the case, the boundary of  $U_4$  is a single geodesic and the Gauss-Bonnet formula implies that

$$\frac{1}{2\pi} \int_{U_4} K dA = 1.\tag{5.7}$$



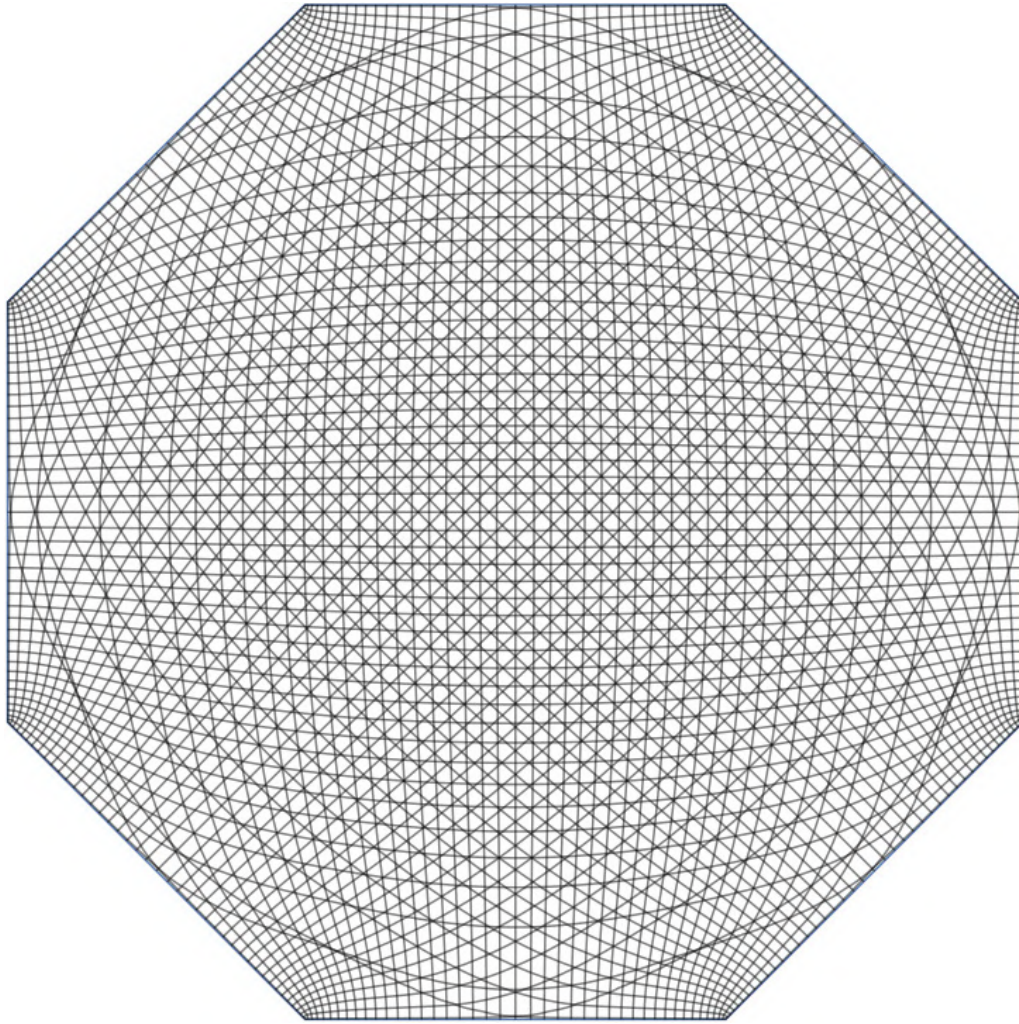


**Figure 9:** The saturating geodesics for the octagon  $P_8$ . The surface is covered by a connected region with four bands of geodesics, eight regions with three bands, and eight regions with two bands.

The ‘dome’  $U_4$  carries the curvature of a half sphere. The union  $U_4 \cup U_3$  is also a topological disk. Its boundary is the outer boundary of  $U_3$  and it is clear that it is also bounded by a smooth geodesic (actually built of sixteen geodesics joining smoothly). Since it is also a disk and we know the bulk integral of curvature over  $U_4$  it follows from Gauss-Bonnet applied to the disk  $U_4 \cup U_3$  that

$$\frac{1}{2\pi} \int_{U_3} K dA + \frac{1}{2\pi} \int_{\partial U_4} k ds = 0. \quad (5.8)$$

Here the second integral is that of the line curvature possibly located on the boundary of  $U_4$ . While we cannot tell the values, it would seem sensible to have negative line curvature on the boundary (as in the hexagon and the Swiss-cross) and positive bulk curvature on  $U_3$ , the two of them canceling exactly. This is of course also needed when we think of extending the disk to the whole surface. As we saw for the hexagon, the inclusion of  $U_2$  does not contribute to the Euler number, for the line curvature on the boundary of  $U_2$  cancels with the corner contribution at the corresponding vertex of the polygon.

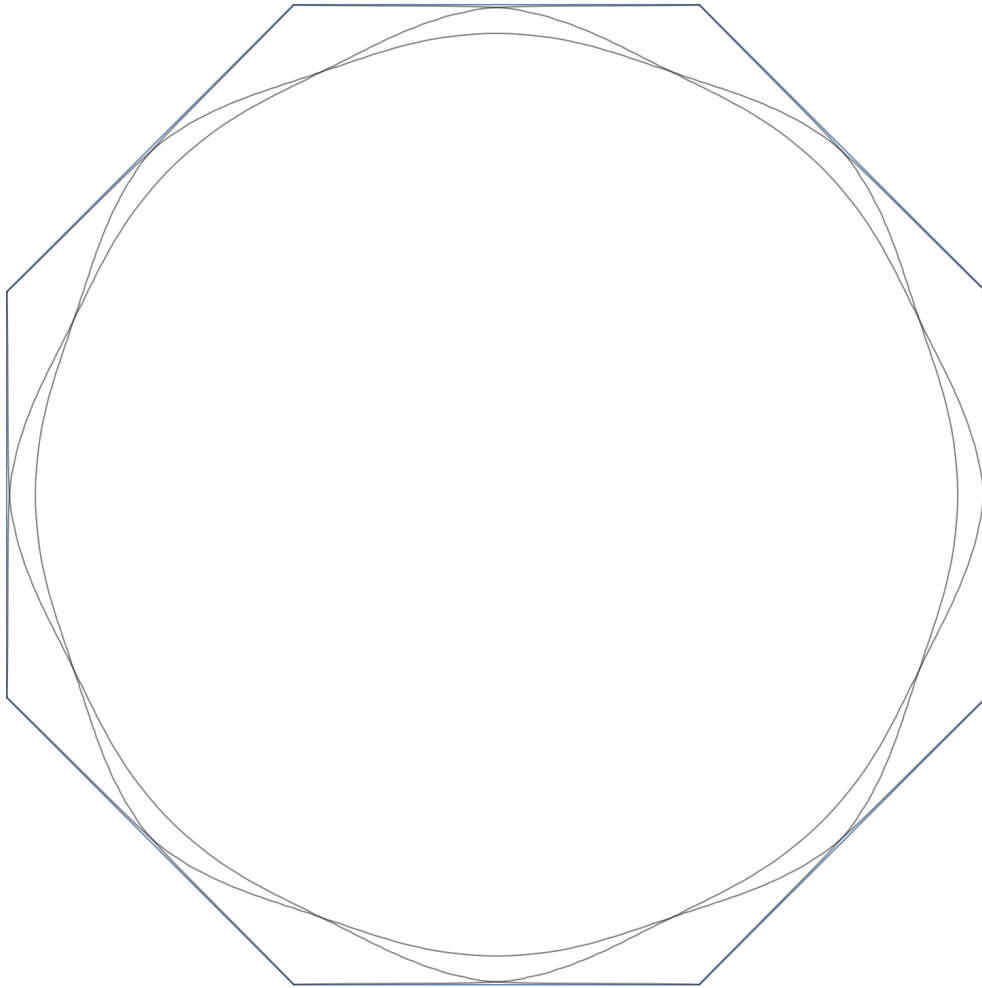


**Figure 10:** The boundary saturating geodesics for  $P_8$ . The surface is covered by a connected region with four bands of geodesics, eight regions with three bands, and eight regions with two bands.

### 5.3 The decagon briefly noted

We can easily apply our program to find the extremal metric on the decagon. The picture of saturating geodesics constructed from our solution is given in Figure 11. In Figure 12 we draw the boundary geodesics in classes  $C_1, C_2, C_3, C_4$ , and  $C_5$ . The region  $U_5$  comprising most of  $P_8$  is covered by five geodesic bands and has positive curvature. As in the previous cases, the boundary of  $U_5$ , clearly visible in Figure 12, is composed of geodesics segments that join without corners. Therefore,

$$\frac{1}{2\pi} \int_{U_5} K dA = 1. \quad (5.9)$$

There are ten small regions of four geodesics. Near each of the edges there is a small region with three geodesics which is bigger than the region with four geodesics. Near each corner we have a flat region with two geodesics.

The best results for area both in the primal program and in the dual program are obtained with  $N_c = 64$ . We have

$$0.7444 < A_{10} < 0.7500. \quad (5.10)$$

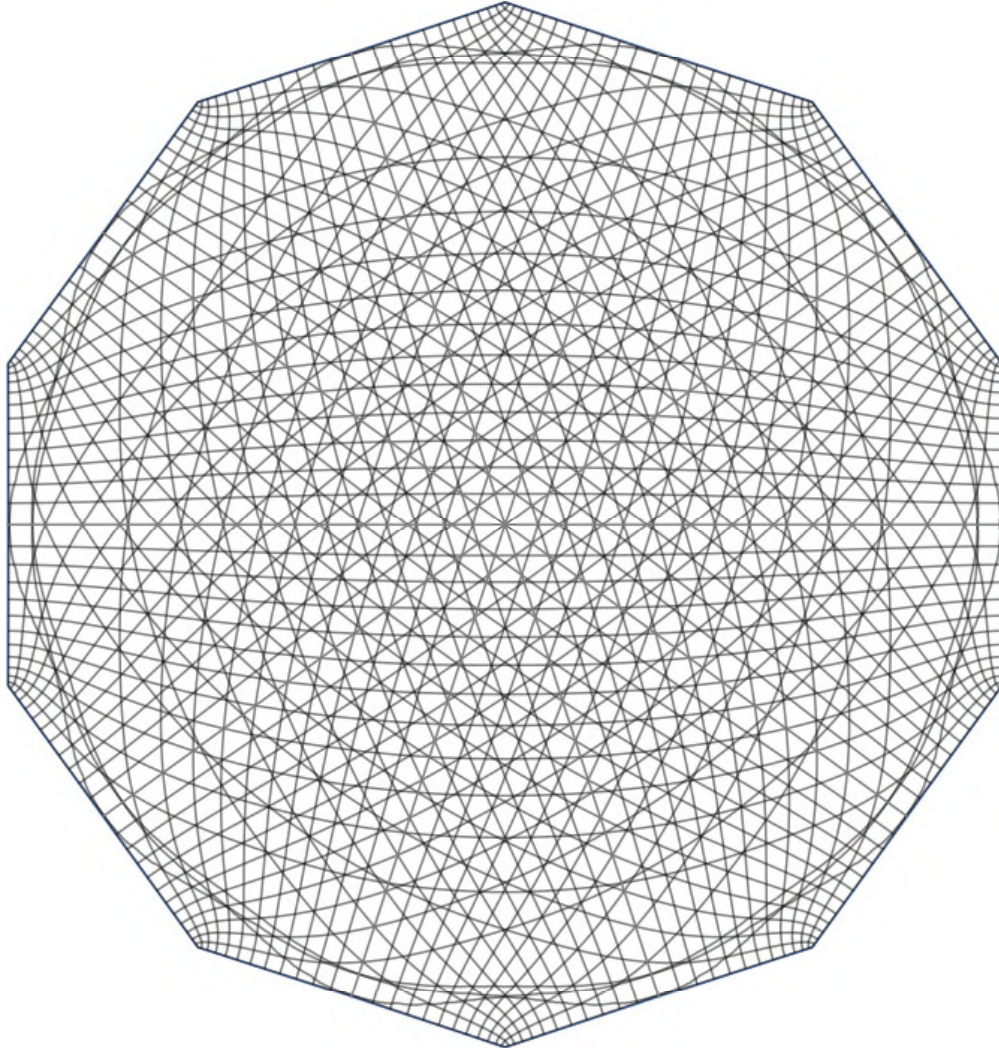


**Figure 11:** The saturating geodesics for  $P_{10}$ . The surface is covered by a connected region with five bands of geodesics, ten regions with four bands, ten regions with three bands and ten regions with two bands.

As in the case of the hexagon and octagon, convergence is faster in the dual program and extrapolation suggests that  $A_{10} = 0.746$ . The flat metric area of the decagon is  $\bar{A}_{10} = \frac{5}{2} \tan(\pi/10) \simeq 0.812299$ . This means that the extremal area is about 8.2% lower than the area of the flat-metric, which is a larger decrease as compared to both the hexagon and the octagon. We also find that the relations  $\mathcal{P}_{10} = 4A_{10}$  and  $A_{10} = 5\nu$  hold very accurately.

## 6 Higher polygons and the extremal metric on $\mathbb{RP}_2$

One can naturally ask for the limit of the extremal metric on  $P_{2n}$  as  $n$  approaches infinity. In this section we review results of Pu [18] and Ahlfors [2] that consider, respectively, the Riemannian and conformal versions of a minimal area problem on a round disk with a length constraint on all curves joining opposite points on the boundary. We study the extremal metrics on  $P_{2n}$  for large  $n$  and

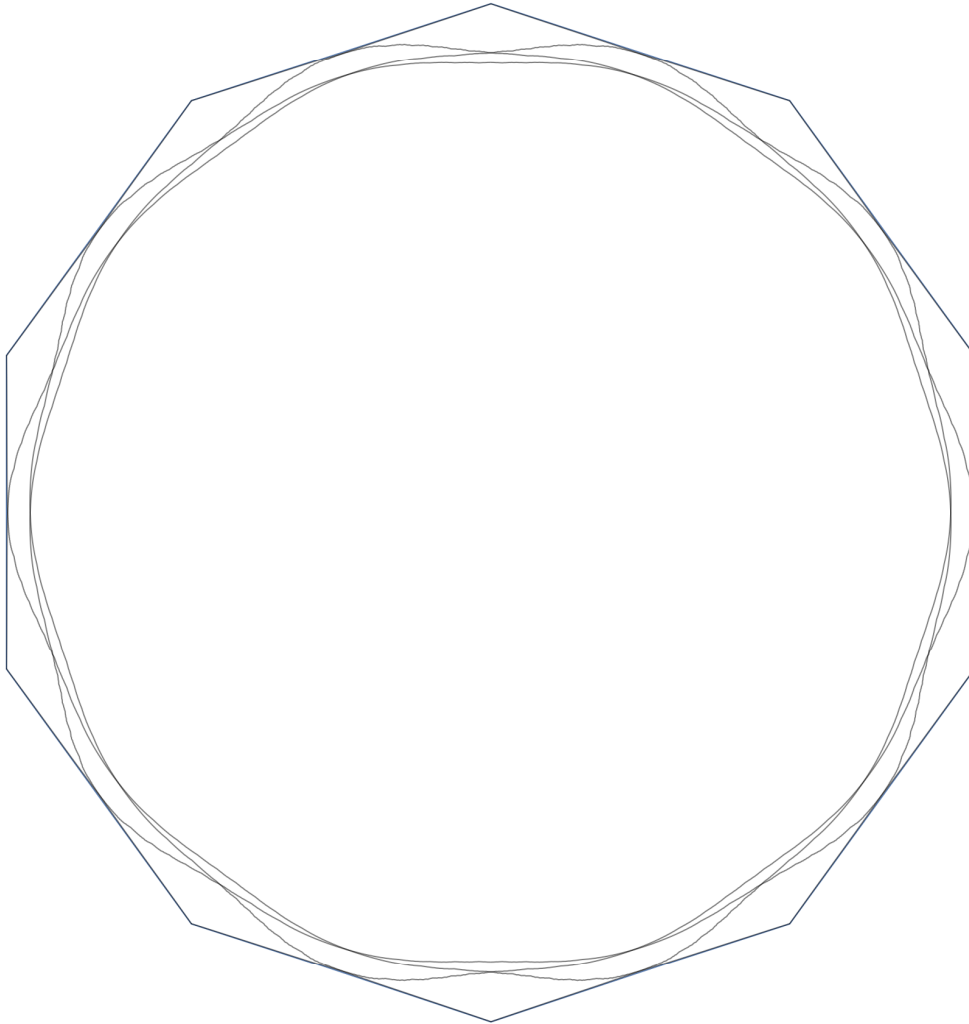


**Figure 12:** The boundary saturating geodesics for  $P_{10}$ . The surface is covered by a connected region  $U_5$ , ten regions comprising  $U_4$ , ten regions comprising  $U_3$  and ten regions comprising  $U_2$ .

conclude that away from the boundary the metrics seem to converge to that of the disk problem.

### 6.1 Riemannian and conformal extremal metrics on $\mathbb{RP}_2$

Among the few minimal area metrics that are explicitly known, that for the real-projective surface  $\mathbb{RP}_2$  in two-dimensions stands out. In this manifold there are non-contractible closed curves and the Riemannian version of the minimal area problem is well defined. The optimal *Riemannian* metric was determined by Pu [18]. The surface with this metric can be described as a round hemisphere with the standard round metric and antipodal points on the circular boundary identified. The problem has also been posed and discussed in the conformal setting [2]. In this version one can consider the disk  $|z| \leq \frac{1}{2}$ , including its boundary, and ask for the minimal area conformal metric such that any curve joining an arbitrary point  $z$  on the boundary to its opposite  $-z$  be longer than or equal to one. The minimal area (conformal) metric is the same as above Riemannian metric; a half-sphere with the round metric. Joining any two antipodal points on the boundary there are infinite systolic geodesics, the set of all great half-circles joining the points. In fact these geodesics

cover the complete hemisphere, and we can think of them as the band of geodesics associated with the pair of points. Furthermore, if we consider the bands of geodesics for *all pairs* of opposite points, we conclude that the surface is in fact covered by an infinite number of bands of geodesics.

With the systole length equal to 1, the radius  $R$  of the half sphere extremal metric is such that the systole  $\pi R$  is equal to one, so

$$R = \frac{1}{\pi}. \quad (6.1)$$

The area  $A$  of the surface in the minimal area metric is

$$A = 2\pi R^2 = \frac{2}{\pi} \simeq 0.63662. \quad (6.2)$$

The systolic area  $\sigma(g)$  for an arbitrary metric  $g$  is defined as the area  $A(g)$  of this metric divided by the square of the systole  $\ell_s(g)$  in this metric:

$$\sigma(g) \equiv \frac{A(g)}{\ell_s^2(g)}. \quad (6.3)$$

The extremal systolic area is the minimal area when the systole is chosen to be equal to one. Pu's result for  $\mathbb{RP}_2$  implies that for any metric  $g$  on this surface

$$\sigma(g) \geq \frac{2}{\pi}. \quad (6.4)$$

As  $n$  becomes large the minimal area problem on  $P_{2n}$  seems to turn into the  $\mathbb{RP}_2$  minimal area problem. Indeed, with apothem fixed at  $\frac{1}{2}$ , as  $n \rightarrow \infty$  the polygon approaches a circular disk of radius  $\frac{1}{2}$ . Moreover, as  $n \rightarrow \infty$  the length condition on curves joining opposite edges seems to become a length condition on curves joining opposite points.

We will show in this section that this intuition is partially correct. We find evidence that the metric on the polygons approaches that of the hemisphere away from the boundary and the area approaches the expected area of a round metric. We find, however, that the perimeter of the polygon does not approach the perimeter of the hemisphere on the round metric. The perimeter in the polygonal case is larger than the perimeter in the round metric. This is presumably due to the local geometry at the (now infinite number of) vertices, where the edges meet orthogonally. Recall the polygon  $P_{2n}$  is covered by regions  $U_2, U_3, \dots, U_n$  and all except  $U_n$  become smaller as  $n \rightarrow \infty$ . It seems plausible that the part of the surface that is the complement of  $U_n$  has vanishing area as  $n \rightarrow \infty$ . While the 'serrated' boundary of the polygon is larger than the perimeter in the round hemisphere, it is also plausible that the length of the boundary of  $U_n$  approaches the perimeter of the round hemisphere as  $n \rightarrow \infty$ .

In order to make comparisons let us consider the metric on a round half-sphere. In unit-free coordinates  $z$  a sphere of radius  $R$  is described by the metric over the full complex plane

$$ds^2 = \frac{4R^2|dz|^2}{(1+|z|^2)^2}, \quad \text{radius } R \text{ sphere with equator } |z| = 1. \quad (6.5)$$

With the north pole at  $z = 0$  and the south pole at  $z = \infty$  one can quickly check that the equator is the curve  $|z| = 1$  and half of the sphere (the northern hemisphere) is the region  $|z| \leq 1$ . Since our polygons  $P_{2n}$  of apothem  $\frac{1}{2}$  converge into the  $|z| \leq \frac{1}{2}$  region as  $n \rightarrow \infty$ , we need to let  $z \rightarrow 2z$  in the above metric to find that

$$ds^2 = \frac{16R^2|dz|^2}{(1+4|z|^2)^2}, \quad \text{radius } R \text{ sphere with equator } |z| = \frac{1}{2}. \quad (6.6)$$

In the conventional notation  $ds^2 = \rho^2|dz|^2$  we read

$$\rho^2(z) = \frac{16R^2}{(1 + 4|z|^2)^2}. \quad (6.7)$$

For the extremal metric with systole equal to one, we saw above that  $R = 1/\pi$ . Therefore, the extremal metric on the disk  $|z| \leq \frac{1}{2}$  is

$$\rho^2(z) = \frac{16}{\pi^2} \frac{1}{(1 + 4|z|^2)^2}. \quad (6.8)$$

In particular, we have that at the origin

$$\rho^2(0) = \frac{16}{\pi^2} \simeq 1.62114. \quad (6.9)$$

## 6.2 Area, perimeter, and metric for large $n$ polygons

We can now use the primal and dual programs to determine the minimal area metrics for the following  $2n$ -gons:

$$2n = 8, 16, 32, 64, 128. \quad (6.10)$$

In each of the polygons we will calculate the relevant quantities for lattice resolution  $N_c = 4, 8, 16, 32$ . Our Mathematica program for the primal succeeded in giving us answers for all these cases. On the other hand the dual program had more trouble and only gave us partial data.

The theoretical prediction (3.36) of the dual program relating area and perimeter for any  $2n$ -gon,

$$\mathcal{P}_{2n} = 4A_{2n}, \quad (6.11)$$

is supported by the data. On the other hand for the extremal metric in  $\mathbb{RP}_2$  (with systole one) we have  $A = 2/\pi$  and perimeter  $\mathcal{P} = 2\pi R = 2$ , giving

$$\mathcal{P} = \pi A, \quad \text{on the extremal metric on } \mathbb{RP}_2. \quad (6.12)$$

The perimeter  $\mathcal{P}_{2n}$  as  $n \rightarrow \infty$  is larger than the one expected in  $\mathbb{RP}_2$ . We believe that the explanation for this is the ‘‘serrated’’ form of the boundary in which, the flat region about the corners of the polygon (in the non-singular metric presentation) has the sides meeting orthogonally. We do not have a detailed model of the polygonal boundary that can explain how to obtain agreement with the area /perimeter relation of the extremal  $\mathbb{RP}_2$ .

Modulo the subtlety associated with  $U_2$  and the corners we find good evidence that the metric converges to the extremal metric on  $\mathbb{RP}_2$  away from the boundary. In Figure 13 we plot the metric along the base of  $T_{2n}$  for various polygons and compare it with the  $\mathbb{RP}_2$  result. It is clear that the metric for higher polygons is converging to the  $\mathbb{RP}_2$  extremal metric.

In Figure 14 we plot the extremal metric for various polygons along the hypotenuse of  $T_{2n}$  and compare it to the extremal  $\mathbb{RP}_2$  metric. We only plot to a fiducial distance of 0.5 from the origin. As we approach the vertex of the polygon the metric starts increasing and then diverges at the vertex. For higher polygons the onset of this divergence shifts closer to the vertex. In the  $n \rightarrow \infty$  limit we expect the metric for polygons to approach the  $\mathbb{RP}_2$  metric everywhere except at the vertex where we encounter a singularity.

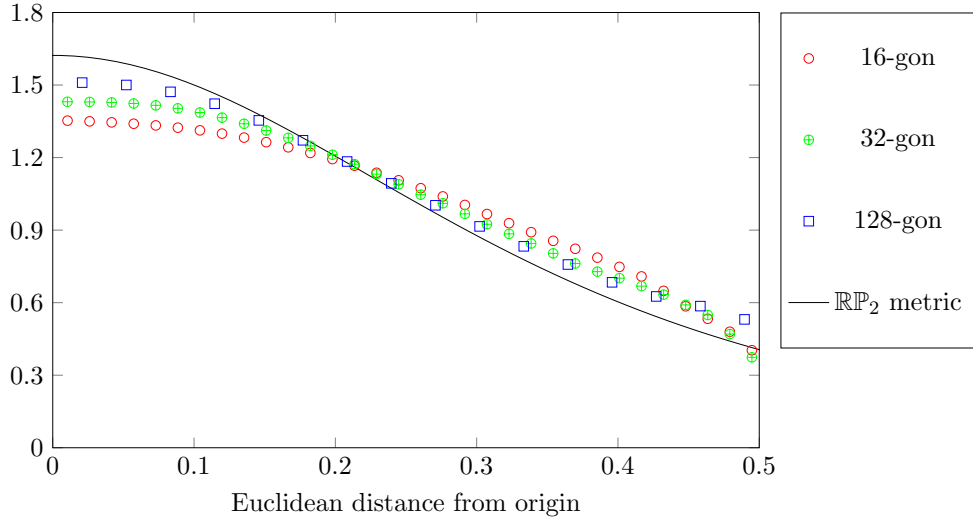


**Figure 13:** Extremal metric along the horizontal axis for various polygons and comparison with the  $\mathbb{RP}_2$  extremal metric. We see evidence of convergence to the  $\mathbb{RP}_2$  metric.

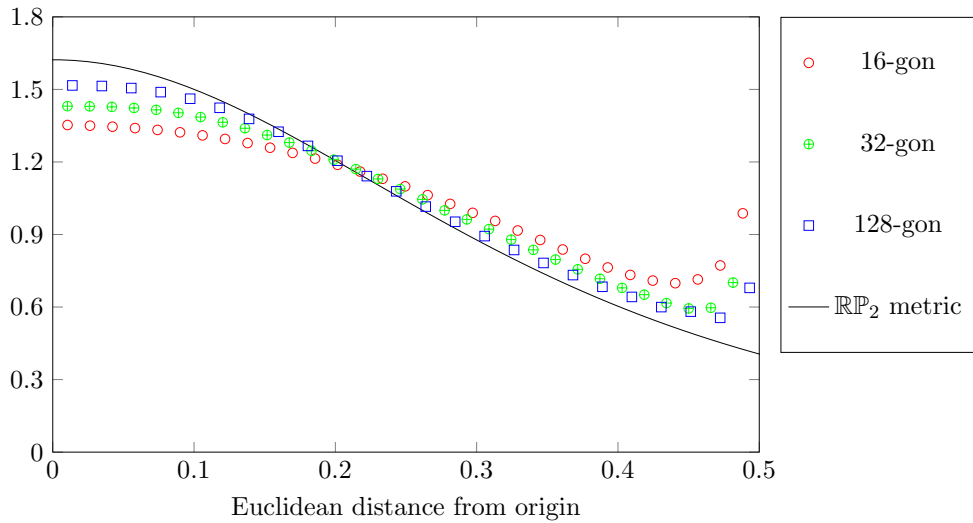


**Figure 14:** Extremal metric along the hypotenuse of  $T_{2n}$  for polygons  $P_{2n}$  and comparison with the extremal metric on  $\mathbb{RP}_2$ . We see evidence of convergence away from the vertex of the polygons.

For the area, extrapolation from the primal gives quantities  $A_{2n}$  that are

$$A_8 = 0.778, \quad A_{16} = 0.700, \quad A_{32} = 0.677, \quad A_{64} = 0.66, \quad A_{128} = 0.654. \quad (6.13)$$

An extrapolation of this suggests  $A_\infty \simeq 0.65$  not far from the minimum in (6.2):  $\frac{2}{\pi} \simeq 0.63662$ . This is evidence that the area is converging to the expected value in the correspondence.

## 7 Conformal metric on $\mathbb{RP}_2$ from the dual program

In this section we demonstrate that the extremal conformal or Riemannian metric on the real projective plane is a critical point of dual variational principle of [14]. This demonstration will entail several challenges, as we will have to deal with a situation in which we have an infinite number of bands of geodesics. As we recall, any two antipodal points determine a band of geodesics that in fact covers the full surface.

### 7.1 Setting up the calculation

We will use the azimuthal angle  $\phi_0$  of a point on the boundary to label the band of geodesics that begins at this point and ends on the antipode  $\phi_0 + \pi$ . Each geodesic on this band is called a  $\phi_0$ -geodesic. For each band we will have coordinates  $x_{\phi_0}$  and  $\varphi_{\phi_0}$ , where the latter is the function that appears in the dual program. Note that  $x_{\phi_0}$  and  $\varphi_{\phi_0}$  are functions all over the sphere, and the geodesics must be lines of constant  $\varphi_{\phi_0}$ .

Our challenge is to find these functions. The function  $x_{\phi_0}$  is the length parameter along  $\phi_0$ -geodesics and is simple to determine. The function  $\varphi_{\phi_0}$  is significantly harder to find because it must satisfy an additional constraint in addition to being constant along geodesics. To explain this, consider the metric using the coordinates  $(x_{\phi_0}, \varphi_{\phi_0})$ , that as explained in [14] takes the form:

$$ds^2 = (dx_{\phi_0})^2 + \frac{1}{h_{\phi_0}^2} (d\varphi_{\phi_0})^2. \quad (7.1)$$

It is not too hard to find a particular function  $\tilde{\varphi}_{\phi_0}$  that, as required, is a constant along the geodesics, as well as the associated  $\tilde{h}_{\phi_0}$  making the above  $ds^2$  the round metric on the hemisphere. The correct  $\varphi_{\phi_0}$ , however, will be a reparameterization of  $\tilde{\varphi}_{\phi_0}$ . As emphasized in [14] (eqn. (7.10)) the various bands  $C_\alpha$  that are active at *any* point on the surface must satisfy the sum rule

$$\sum_{\alpha} |d\varphi^\alpha| = 1. \quad (7.2)$$

Here  $\alpha$  labels the active bands at any point. In our case the role of the index  $\alpha$  is played by the continuous variable  $\phi_0 \in [0, \pi]$ . Still using the sum notation, we have

$$\sum_{\phi_0} |d\varphi_{\phi_0}| = 1. \quad (7.3)$$

The form (7.1) of the metric implies that  $|d\varphi_{\phi_0}| = |h_{\phi_0}|$  and therefore the sum rule becomes

$$\sum_{\phi_0} |h_{\phi_0}| = 1. \quad (7.4)$$

The left hand side is a function over the surface, but that function must be a constant. Under a reparameterization  $\varphi_{\phi_0} \rightarrow \tilde{\varphi}_{\phi_0}(\varphi_{\phi_0})$  the metric invariance requires

$$\frac{|d\varphi_{\phi_0}|}{|h_{\phi_0}|} = \frac{|d\tilde{\varphi}_{\phi_0}|}{|\tilde{h}_{\phi_0}|} \rightarrow |h_{\phi_0}| = |\tilde{h}_{\phi_0}| \left| \frac{d\varphi_{\phi_0}}{d\tilde{\varphi}_{\phi_0}} \right|. \quad (7.5)$$

Since the function  $h_{\phi_0}$  transforms nontrivially under a  $\varphi_{\phi_0}$  reparameterization, it is clear that if an original choice of  $\varphi_{\phi_0}$  does not make the sum rule (7.4) work, a reparameterization of it may.



To find the continuous form of the sum rule we imagine working with a polygon with  $2n$  sides, and thus  $n$  foliations, in the limit of large  $n$ . We will take  $n$  equally spaced values of  $\phi_0$  in the range from 0 to  $\pi$ . With this discretization the sum rule becomes

$$\sum_{k=1}^n |h_{\phi_k}| = 1, \quad \text{with} \quad \phi_k = k \frac{\pi}{n}, \quad k = 1, \dots, n. \quad (7.6)$$

Passing to an integral is done by multiplying the above equation by  $\Delta\phi = \frac{\pi}{n}$

$$\sum_{k=1}^n |h_{\phi_k}| \Delta\phi = \frac{\pi}{n}. \quad (7.7)$$

For very large  $n$ , using a continuous  $\phi_0 \in (0, \pi)$ , we have the integral constraint:

$$\int_0^\pi d\phi_0 |h_{\phi_0}| \simeq \frac{\pi}{n}, \quad n \gg 1. \quad (7.8)$$

This is our main constraint. The most nontrivial part is ensuring that the integral over all the bands of the position dependent  $|h_{\phi_0}|$  is a constant over the sphere. After that is done, there is the issue of the constant being equal to the constant on the right-hand side. This will require finding the value of the height function  $\nu$  as a function of  $n$ , for large  $n$ . This value of  $\nu$  must be such that the correct area of the surface is obtained from the large  $n$  limit of  $n\nu$  as explained in (3.23).

## 7.2 Working out the details

In this section  $z = x + iy$  is the complex coordinate in which the disk is  $|z| \leq \frac{1}{2}$ . With radius  $R = 1/\pi$ , corresponding to a systole of 1, the metric (6.8) is:

$$ds^2 = \frac{16}{\pi^2} \frac{|dz|^2}{(1 + 4|z|^2)^2}, \quad |z| \leq \frac{1}{2}, \quad z = x + iy. \quad (7.9)$$

To use some of the previously derived results, we must relate these  $(x, y)$  coordinates to the cartesian coordinates  $\hat{x}, \hat{y}$  defined as usual from the spherical angles  $\theta, \phi$  and the radius  $R$ :

$$\begin{aligned} \hat{x} &= R \sin \theta \cos \phi, \\ \hat{y} &= R \sin \theta \sin \phi. \end{aligned} \quad (7.10)$$

One can easily show that for  $R = 1/\pi$ , our case of interest, the two sets of coordinates are related as follows:

$$\hat{x} = \frac{1}{\pi} \frac{4x}{1 + 4|z|^2}, \quad \hat{y} = \frac{1}{\pi} \frac{4y}{1 + 4|z|^2}. \quad (7.11)$$

One can also prove the useful identities:

$$1 + 4(x^2 + y^2) = \sec^2 \frac{\theta}{2}, \quad \cos \theta = \frac{1 - 4|z|^2}{1 + 4|z|^2}. \quad (7.12)$$

Defining coordinates for the band labelled by  $\phi_0$ . On the round hemisphere of radius  $1/\pi$  representing the extremal metric with systole one, we can consider the so-called  $\phi_0$ -geodesics that begin on the equator at  $\phi_0$  and end on the equator at  $\phi_0 + \pi$ . They comprise a band of geodesics that covers

the full hemisphere. Using coordinates  $\theta$  and  $\phi$  on the sphere,  $x_{\phi_0}$  is a coordinate that parameterizes these geodesics by length. In Figure 15, the geodesic starts at point  $u$ , corresponding to  $\phi_0$  and ends at  $v$ , corresponding to  $\phi_0 + \pi$ . The point  $P$  lies on a geodesic joining  $u$  and  $v$  and has spherical coordinates  $(\phi, \theta)$ . The length of the geodesic arc connecting  $u$  and  $P$  is then equal to  $x_{\phi_0}$  at  $P$ . This arc length can be expressed in terms of the radius  $1/\pi$  of the sphere and the angle  $\Delta\sigma$  shown

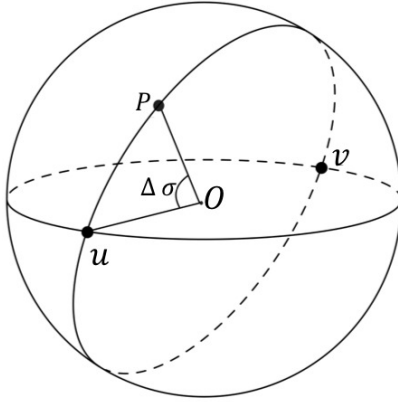


**Figure 15:** A geodesic joining antipodal points  $u$  and  $v$  on the equator.

in the figure:

$$x_{\phi_0} = \Delta\sigma/\pi. \quad (7.13)$$

Let us denote by  $P$  and  $u$  the vectors from origin to points  $P$  and  $u$  respectively

$$P = \frac{1}{\pi} (\sin \theta \cos \phi, \sin \theta \sin \phi, \cos \theta), \quad u = \frac{1}{\pi} (\cos \phi_0, \sin \phi_0, 0). \quad (7.14)$$

The angle  $\Delta\sigma$  is then given by

$$\cos \Delta\sigma = \frac{P \cdot u}{|P||u|} = \sin \theta \cos(\phi - \phi_0). \quad (7.15)$$

The coordinate  $x_{\phi_0}(\theta, \phi)$  is just the arc-length:

$$x_{\phi_0}(\theta, \phi) = \frac{1}{\pi} \cos^{-1}(\sin \theta \cos(\phi - \phi_0)). \quad (7.16)$$

We thus have

$$\cos \pi x_{\phi_0}(\theta, \phi) = (\sin \theta \cos(\phi - \phi_0)). \quad (7.17)$$

In terms of the disk coordinates  $(x, y)$ , this is

$$\cos \pi x_{\phi_0} = \frac{4(x \cos \phi_0 + y \sin \phi_0)}{1 + 4|z|^2}. \quad (7.18)$$

Let us find the second coordinate  $\tilde{\varphi}_{\phi_0}$ . This coordinate must be such that each  $\phi_0$  geodesic is a curve of constant  $\tilde{\varphi}_{\phi_0}$ . Geodesics on the sphere are great circles which can be parameterized by a constant  $c$  and an angle  $\phi_0$  as follows

$$\cot \theta = c \sin(\phi - \phi_0). \quad (7.19)$$

At the equator we have latitude  $\theta = \frac{\pi}{2}$ , the left-hand side vanishes and the right-hand side implies that the geodesic meets the equator at the azimuthal angles  $\phi = \phi_0$  and  $\phi_0 + \pi$ . Now consider

following the geodesic as  $\phi$  increases from the value  $\phi_0$ . The latitude angle  $\theta$  decreases from  $\pi/2$  and reaches a minimum when the right-hand side is a maximum at  $\phi = \phi_0 + \frac{\pi}{2}$ . This minimum latitude will be the searched for  $\tilde{\varphi}_{\phi_0}$ . This implies  $\cot \tilde{\varphi}_{\phi_0} = c$  and the equation of the geodesic is

$$\cot \theta = \cot \tilde{\varphi}_{\phi_0} \sin(\phi - \phi_0) . \quad (7.20)$$

For our problem we only consider geodesics on the upper hemisphere. For a chosen  $\phi_0$  these fall into two classes, separated by the great circle going through the north pole: those that are lifts of the half-circle  $\phi \in [\phi_0, \phi_0 + \pi]$  and those that are lifts of the half circle  $\phi \in [\phi_0 + \pi, \phi_0 + 2\pi]$ . Since the left-hand side of (7.20) must always be positive to be on the upper hemisphere,  $\cot \tilde{\varphi}_{\phi_0}$  must alternate sign in the two classes and will range in the interval

$$\tilde{\varphi}_{\phi_0} \in \left(-\frac{\pi}{2}, \frac{\pi}{2}\right) . \quad (7.21)$$

For our conventions it will be useful to alter the sign in (7.20) and to have

$$\cot \theta = -\cot \tilde{\varphi}_{\phi_0} \sin(\phi - \phi_0) . \quad (7.22)$$

This amounts to just changing the role of the two classes of curves. From this it follows that

$$\tan \tilde{\varphi}_{\phi_0} = -\tan \theta \sin(\phi - \phi_0) . \quad (7.23)$$

This formula displays  $\tilde{\varphi}_{\phi_0}$  as a function that is constant over each geodesic half circle. One can quickly show that in the disk coordinates  $(x, y)$  this becomes

$$\tilde{\varphi}_{\phi_0} = -\tan^{-1}\left(\frac{4(y \cos \phi_0 - x \sin \phi_0)}{1 - 4|z|^2}\right) . \quad (7.24)$$

Calculating the metric in the  $x_{\phi_0}$  and  $\tilde{\varphi}_{\phi_0}$  coordinates.

We have now expressions for  $x_{\phi_0}$  and  $\tilde{\varphi}_{\phi_0}$ . To find  $dx_{\phi_0}$  we take the differential of equation (7.18). A little computation gives

$$-\frac{\pi}{4} \sin(\pi x_{\phi_0}) dx_{\phi_0} = \frac{\alpha dx + \beta dy}{(1 + 4|z|^2)^2} . \quad (7.25)$$

Here we have defined the functions  $\alpha$  and  $\beta$  as follows:

$$\begin{aligned} \alpha &= (1 + 4(y^2 - x^2)) \cos \phi_0 - 8xy \sin \phi_0 , \\ \beta &= (1 + 4(y^2 - x^2)) \sin \phi_0 - 8xy \cos \phi_0 . \end{aligned} \quad (7.26)$$

A quantity that will appear many times is  $\alpha^2 + \beta^2$ , which can be written in four useful ways:

$$\begin{aligned} \alpha^2 + \beta^2 &= 1 + 16|z|^4 - 8[(x^2 - y^2) \cos 2\phi_0 + 2xy \sin 2\phi_0] , \\ &= (1 - 4|z|^2)^2 + 16(y \cos \phi_0 - x \sin \phi_0)^2 , \\ &= (1 + 4|z|^2)^2 - 16(x \cos \phi_0 + y \sin \phi_0)^2 , \\ &= (e^{i\phi_0} - 4z^2 e^{-i\phi_0})(e^{-i\phi_0} - 4\bar{z}^2 e^{i\phi_0}) , \end{aligned} \quad (7.27)$$

with

$$e^{i\phi_0} - 4z^2 e^{-i\phi_0} = \alpha + i\beta . \quad (7.28)$$

Calculation of  $d\tilde{\varphi}_{\phi_0}$  from (7.24) takes a little work, and with the use of (7.27) gives

$$d\tilde{\varphi}_{\phi_0} = \frac{4(\beta dx - \alpha dy)}{\alpha^2 + \beta^2}. \quad (7.29)$$

The metric function  $\tilde{h}_{\phi_0}$  can be obtained from the general relation between calibrations and  $\varphi$  functions [14]:

$$u^\alpha = -\frac{*d\varphi^\alpha}{|d\varphi^\alpha|}. \quad (7.30)$$

For our case this reads:

$$dx_{\phi_0} = -\frac{*d\tilde{\varphi}_{\phi_0}}{|d\tilde{\varphi}_{\phi_0}|}. \quad (7.31)$$

Since  $|d\tilde{\varphi}_{\phi_0}| = |\tilde{h}_{\phi_0}|$  when we write the metric as

$$ds^2 = (dx_{\phi_0})^2 + \frac{1}{\tilde{h}_{\phi_0}^2} (d\tilde{\varphi}_{\phi_0})^2, \quad (7.32)$$

we find

$$*d\tilde{\varphi}_{\phi_0} = -|\tilde{h}_{\phi_0}| dx_{\phi_0}. \quad (7.33)$$

Using the earlier calculation of  $d\tilde{\varphi}_{\phi_0}$  and  $dx_{\phi_0}$  and recalling that  $*(adx + bdy) = -bdx + ady$ , we get

$$|h_{\phi_0}| = \pi \sin(\pi x_{\phi_0}) \frac{(1 + 4|z|^2)}{\alpha^2 + \beta^2}. \quad (7.34)$$

This can be simplified. Indeed, a short calculation shows that

$$\frac{(1 + 4|z|^2)}{\alpha^2 + \beta^2} = \frac{1}{(\sin \pi x_{\phi_0})^2}, \quad (7.35)$$

giving

$$|\tilde{h}_{\phi_0}| = \frac{\pi}{\sin \pi x_{\phi_0}}. \quad (7.36)$$

The metric (7.32) is therefore given by

$$ds^2 = (dx_{\phi_0})^2 + \frac{1}{\pi^2} (\sin \pi x_{\phi_0})^2 (d\tilde{\varphi}_{\phi_0})^2. \quad (7.37)$$

Thinking of the origin of the  $\phi_0$  geodesics as a new north pole, we can see that  $\pi x_{\phi_0} \in [0, \pi]$  is in fact the relevant polar angle  $\tilde{\theta}_{\phi_0}$ . With this the metric takes the form

$$ds^2 = R^2 [(d\tilde{\theta}_{\phi_0})^2 + \sin^2 \tilde{\theta}_{\phi_0} (d\tilde{\varphi}_{\phi_0})^2], \quad R = 1/\pi. \quad (7.38)$$

This is clearly the expected round metric on the hemisphere. While we had defined  $\tilde{\varphi}_{\phi_0}$  as the minimum latitude of the geodesic, in this picture  $\tilde{\varphi}_{\phi_0}$  is seen equivalently to be an azimuthal angle. The function  $\tilde{\varphi}_{\phi_0}$  that labels the various  $\phi_0$  geodesics is the departure angle at the origin  $x_{\phi_0} = 0$ . This is clearly a natural variable and its range  $(-\frac{\pi}{2}, \frac{\pi}{2})$  (see (7.21)) is consistent with this interpretation. Here  $\tilde{\varphi}_{\phi_0} = 0$  labels the geodesic departing orthogonal to the boundary.

#### Reparameterization and final steps.

A little experimentation shows that the function  $|\tilde{h}_{\phi_0}|$  does not satisfy the sum rule constraint (7.8): the integral on the left-hand side fails to be position independent on the surface. As explained

before, the definitive coordinate  $\varphi$  is to be obtained by a reparameterization of  $\tilde{\varphi}$ . A bit of trial and error quickly led to a satisfactory solution:

$$\varphi_{\phi_0} = \frac{\nu}{2} \sin \tilde{\varphi}_{\phi_0}, \quad \varphi_{\phi_0} \in \left(-\frac{\nu}{2}, \frac{\nu}{2}\right). \quad (7.39)$$

By setting the coefficient equal to  $\nu/2$  we guarantee that function has the required discontinuity by  $\nu$ : the top-most and bottom-most geodesic in the band are identified, and on those the function  $\varphi$  takes values  $\nu/2$  and  $-\nu/2$ ). Using (7.5) we have

$$|h_{\phi_0}| = |\tilde{h}_{\phi_0}| \left| \frac{d\varphi_{\phi_0}}{d\tilde{\varphi}_{\phi_0}} \right| = \frac{\pi\nu}{2} \frac{\cos \tilde{\varphi}_{\phi_0}}{\sin \pi x_{\phi_0}}. \quad (7.40)$$

This result simplifies considerably when referred to  $(x, y)$  coordinates. All square roots disappear and we find

$$|h_{\phi_0}| = \frac{\pi\nu}{2} \cdot \frac{1 - 16|z|^4}{1 + 16|z|^4} \cdot \frac{1}{1 - a \cos 2\phi_0 - b \sin 2\phi_0}, \quad (7.41)$$

with:

$$a \equiv \frac{8(x^2 - y^2)}{1 + 16|z|^4}, \quad b \equiv \frac{16xy}{1 + 16|z|^4}, \quad (7.42)$$

With this value of  $|h_{\phi_0}|$  the constraint (7.8) becomes

$$\frac{\pi\nu}{2} \cdot \frac{1 - 16|z|^4}{1 + 16|z|^4} \int_0^\pi \frac{d\phi_0}{1 - a \cos 2\phi_0 - b \sin 2\phi_0} \simeq \frac{\pi}{n}. \quad (7.43)$$

The left hand side must be  $z$  independent for this to work. The integral is readily evaluated giving:

$$\int_0^\pi \frac{d\phi_0}{1 - a \cos 2\phi_0 - b \sin 2\phi_0} = \frac{\pi}{\sqrt{1 - (a^2 + b^2)}} = \pi \cdot \frac{1 + 16|z|^4}{1 - 16|z|^4}. \quad (7.44)$$

As a result, the  $z$  dependence of the left-hand side of (7.43) disappears and we are left with

$$\frac{\pi\nu}{2} \pi \simeq \frac{\pi}{n} \quad \rightarrow \quad \nu = \frac{2}{\pi n}. \quad (7.45)$$

With this choice of  $\nu$  we satisfy the constraint for large  $n$ . Recall that the area functional at the critical point is  $A = \sum_{k=1}^n \nu_k \ell_s$ . By symmetry, all  $\nu_k$  parameters are to  $\nu$ , and having set  $\ell_s = 1$ , we have

$$A = n\nu = n \cdot \frac{2}{\pi n} = \frac{2}{\pi}. \quad (7.46)$$

This is the correct value for the extremal area  $A = 2\pi R^2 = 2\pi/\pi^2 = 2/\pi$ . This shows that we have a maximum of the dual functional in the limit  $n \rightarrow \infty$ , and it reproduces the expected result.

In order to understand better the solution we consider a few figures. In Figure 16 we show the azimuthal departure angles for  $\phi_0$  geodesics leaving the boundary point  $x_{\phi_0} = 0$ , placed at the origin of the figure. For  $\tilde{\varphi}_{\phi_0}$ , geodesics must be imagined leaving at equal intervals of this variable. This is shown to the left: since  $\tilde{\varphi}_{\phi_0}$  is the azimuthal angle relative to the departing point, the geodesics are uniformly distributed in the interval  $(-\frac{\pi}{2}, \frac{\pi}{2})$ . To the right, we show the geodesics, for the final dual coordinate  $\varphi_{\phi_0} \sim \sin(\tilde{\varphi}_{\phi_0})$ . Here geodesics equally spaced in this variable are not equally spaced azimuthally. They are squeezed near the vertical axis and are set apart near the boundary.

In Figure 17 we consider again the solution for a single band of systolic geodesics described by coordinates  $(x_{\phi_0}, \varphi_{\phi_0})$  with  $\phi_0 = 0$  so that the antipodal points lie on the real axis of the  $|z| \leq \frac{1}{2}$  disk. To the left we show the function  $|h_{\phi_0=0}|$ , which using (7.41) is proportional to

$$|h_0| \sim \frac{1 - 16(x^2 + y^2)^2}{1 - 8(x^2 - y^2) + 16(x^2 + y^2)^2}. \quad (7.47)$$

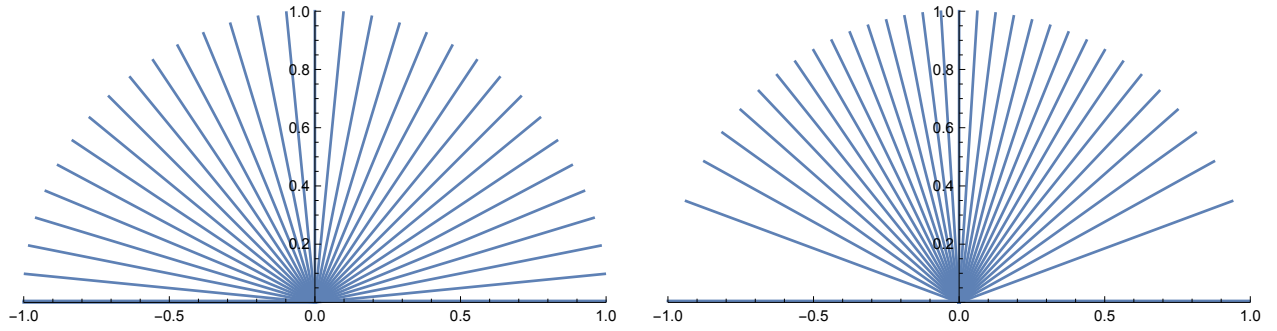


**Figure 16:** A closeup of  $\phi_0$  geodesics as they depart  $x_{\phi_0} = 0$ , placed at the origin of the figure. The boundary is represented by the horizontal lines. Left: With  $\tilde{\varphi}_{\phi_0}$  the geodesics depart at identically spaced azimuthal angles. Right: With  $\varphi_{\phi_0}$  the geodesics are squeezed around the vertical axis and are separated out near the boundary.

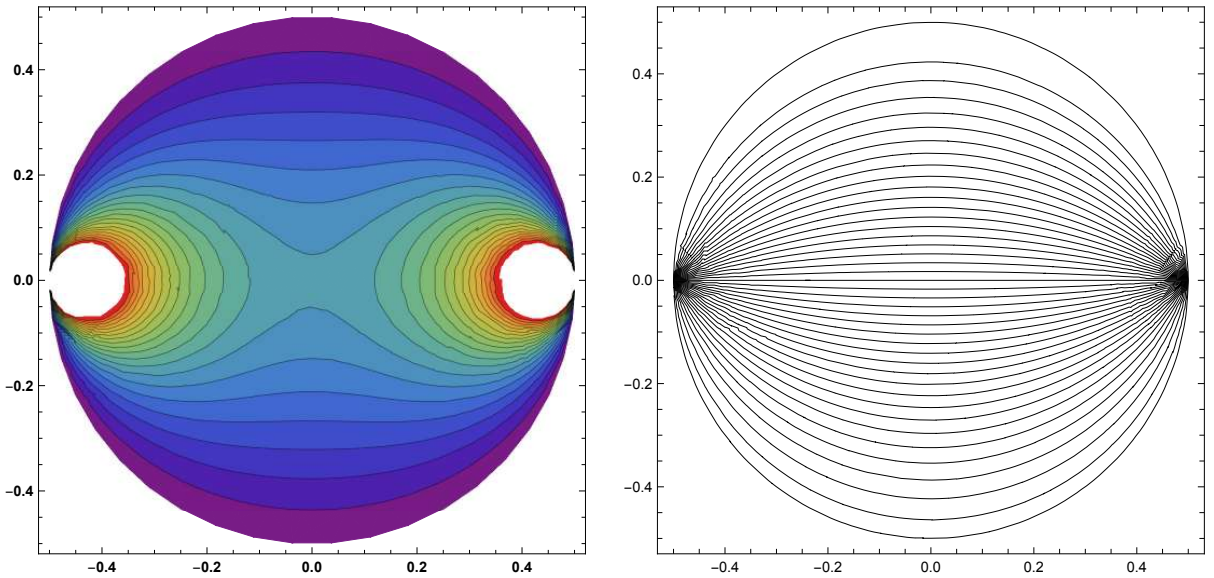


**Figure 17:** Left: Contour plot of  $|h_{\phi_0}|$  (with  $\phi_0 = 0$ ) defining the density of systolic geodesics on the  $|z| \leq \frac{1}{2}$  disk. Right: Systolic geodesics at equal spacings of the coordinate  $\varphi_{\phi_0}$  that labels them.

The function  $|h_{\phi_0}|$  has the interpretation of density of geodesics, or number of geodesics per unit transverse length in the convention that geodesics are spaced by equal amounts in the  $\varphi_{\phi_0}$  coordinate [14]. This density function is singular at the departing and ending points  $(\frac{1}{2}, 0)$  and  $(-\frac{1}{2}, 0)$  where it becomes infinite as approached from the interior. The function  $|h|$  vanishes at the rest of the boundary. To the right we show the geodesics themselves, plotted on the  $z$ -disk for equal spacings of the  $\varphi_{\phi_0}$  coordinate. Recall that the  $(x, y)$  coordinates on the disk are nontrivially related to the Cartesian coordinates  $(\hat{x}, \hat{y})$ , that together with  $\hat{z}$  describe the hemisphere as  $\hat{x}^2 + \hat{y}^2 + \hat{z}^2 = 1/\pi^2$ , with  $\hat{z} \geq 0$ .

## 8 Calabi's variational principle

In this section we review the variational principle put forth by Calabi [13] to deal with regions covered by three bands of systolic geodesics and give the associated Euler-Lagrange equations. This variational principle was further investigated in reference [17], that proposed an extension to deal with regions covered by more than three bands of systolic geodesics. We find, however, some difficulties with the proposal and its conclusions. We show that the bands of geodesics relevant to the metric on  $\mathbb{RP}_2$  do not satisfy the anticipated equation of motion. We will give our modified variational principle in section 9.

### 8.1 The variational principle for regions with three systolic bands

Calabi considered the extremal isosystolic metric in a region  $U_3$  covered by exactly three bands of geodesics, each band calibrated by a closed one-form of unit norm. Locally, the calibrating one-form can be written as the differential of the length parameter that Calabi calls 'geodesic potential function'. The calibrating one-forms are thus given by  $u^\alpha = dX^\alpha$ , with  $\alpha = 1, 2, 3$ . We take  $(X, Y) \equiv (X^1, X^2)$  as coordinates on  $U_3$  and consider the third geodesic potential  $Z \equiv X^3$  as a function  $Z(X, Y)$  of the coordinates. In coordinates  $(X, Y)$ , the condition that  $u^1 = dX$  and  $u^2 = dY$  are one-forms of unit norm fixes the cotangent space metric  $g^{-1}$  to be:

$$g^{-1} = \begin{pmatrix} 1 & f \\ f & 1 \end{pmatrix}. \quad (8.1)$$

Here  $f$  is a function that appears in the inner product of  $dX$  and  $dY$ :

$$\langle u^1, u^2 \rangle = \langle dX, dY \rangle = f = \langle \hat{u}^1, \hat{u}^2 \rangle. \quad (8.2)$$

Here  $\hat{u}^1$  and  $\hat{u}^2$  are the unit vectors associated to the one forms  $u^1$  and  $u^2$ , defined as usual by the relation  $u^i(v) = \langle \hat{u}^i, v \rangle$ , with  $v$  an arbitrary vector. Since the unit vectors  $\hat{u}^1$  and  $\hat{u}^2$  are, respectively, tangent to the first and second band of geodesics, their inner product is simply the cosine of the angle  $\theta_{12}$  between these first two geodesic bands:

$$\cos \theta_{12} = f. \quad (8.3)$$

This is the interpretation of  $f$ . When  $f$  vanishes the bands associated with  $X$  and  $Y$  are orthogonal. We also require the last one form,  $u^3 = dZ$  be of unit magnitude. For this we note that

$$dZ = Z_X dX + Z_Y dY, \quad Z_X \equiv \frac{\partial Z}{\partial X}, \quad Z_Y \equiv \frac{\partial Z}{\partial Y}. \quad (8.4)$$

Then the norm equal one condition gives

$$|dZ|^2 = \langle dZ, dZ \rangle = Z_X^2 + Z_Y^2 + 2f Z_X Z_Y = 1. \quad (8.5)$$

We can now solve for  $f$  in terms of derivatives of the potential  $Z$ :

$$f = \frac{1 - Z_X^2 - Z_Y^2}{2 Z_X Z_Y}, \quad (8.6)$$

showing that the existence of the third band determines the metric. Associated with the cotangent metric  $g^{-1}$  above the metric  $g$  is

$$g = \frac{1}{1-f^2} \begin{pmatrix} 1 & -f \\ -f & 1 \end{pmatrix} \rightarrow \sqrt{\det g} = \frac{1}{\sqrt{1-f^2}}. \quad (8.7)$$

The variational principle posits that the area, defined as the integral  $I$  of the area form  $\sqrt{\det g} dX \wedge dY$ , is stationary under *local* variations  $\delta Z$  of the potential  $Z$  for the third band. The local variation, by definition does not change the period of the potential, which controls the total length of the geodesics. We thus have

$$I = \int_{U_3} L(Z_X, Z_Y) dX \wedge dY, \quad L = \frac{2|Z_X Z_Y|}{\sqrt{(2Z_X Z_Y)^2 - (Z_X^2 + Z_Y^2 - 1)^2}}. \quad (8.8)$$

The Euler-Lagrange equation is readily obtained and takes the form

$$\frac{\partial}{\partial X} \left[ \frac{\partial L}{\partial Z_X} \right] + \frac{\partial}{\partial Y} \left[ \frac{\partial L}{\partial Z_Y} \right] = 0. \quad (8.9)$$

To get an explicit version we first find that

$$\begin{aligned} \frac{\partial L}{\partial Z_X} &= [Z_X^4 - (Z_Y^2 - 1)^2] \frac{2Z_Y}{\Delta^{3/2}}, \\ \frac{\partial L}{\partial Z_Y} &= [Z_Y^4 - (Z_X^2 - 1)^2] \frac{2Z_X}{\Delta^{3/2}}, \end{aligned} \quad (8.10)$$

where we defined

$$\Delta \equiv (2Z_X Z_Y)^2 - (Z_X^2 + Z_Y^2 - 1)^2. \quad (8.11)$$

The final form of the differential equation is long, but worth recording<sup>3</sup>:

$$f(Z_X, Z_Y) Z_{XX} + g(Z_X, Z_Y) Z_{XY} + \tilde{f}(Z_X, Z_Y) Z_{YY} = 0, \quad (8.12)$$

where  $f, g$ , and  $\tilde{f}$  are functions of  $Z_X$  and  $Z_Y$  that ordered by the number of derivatives take the form

$$\begin{aligned} f &= Z_X Z_Y (3 - 5Z_X^2 - 3Z_Y^2 + Z_X^4 + 10Z_X^2 Z_Y^2 - 3Z_Y^4 + Z_X^6 + Z_X^4 Z_Y^2 - 5Z_X^2 Z_Y^4 + 3Z_Y^6), \\ g &= 1 - 2Z_X^2 - 2Z_Y^2 + 16Z_X^2 Z_Y^2 + 2Z_X^6 - 10Z_X^4 Z_Y^2 - 10Z_X^2 Z_Y^4 + 2Z_Y^6 \\ &\quad - Z_X^8 - 4Z_X^6 Z_Y^2 + 10Z_X^4 Z_Y^4 - 4Z_X^2 Z_Y^6 - Z_Y^8, \\ \tilde{f} &= Z_X Z_Y (3 - 5Z_Y^2 - 3Z_X^2 + Z_Y^4 + 10Z_X^2 Z_Y^2 - 3Z_X^4 + Z_Y^6 + Z_X^2 Z_Y^4 - 5Z_X^4 Z_Y^2 + 3Z_X^6). \end{aligned} \quad (8.13)$$

We note that

$$\tilde{f}(Z_X, Z_Y) = f(Z_Y, Z_X), \quad \text{and} \quad g(Z_X, Z_Y) = g(Z_Y, Z_X). \quad (8.14)$$

## 8.2 Connecting the conformal and isosystolic formalisms

Our numerical results for the hexagon (section 4) can be used to obtain the potential functions  $X^1, X^2, X^3$  and to describe the area form in terms of these coordinates. The coordinate  $X^\alpha$  attains the value  $-\frac{1}{2}$  on the edge  $e_\alpha$  and  $+\frac{1}{2}$  on the edge  $\tilde{e}_\alpha$ , as shown for  $P_6$  in Figure 18.

<sup>3</sup>We have dropped an overall factor of  $\frac{4}{\Delta^{5/2}}$  in arriving at this final form.



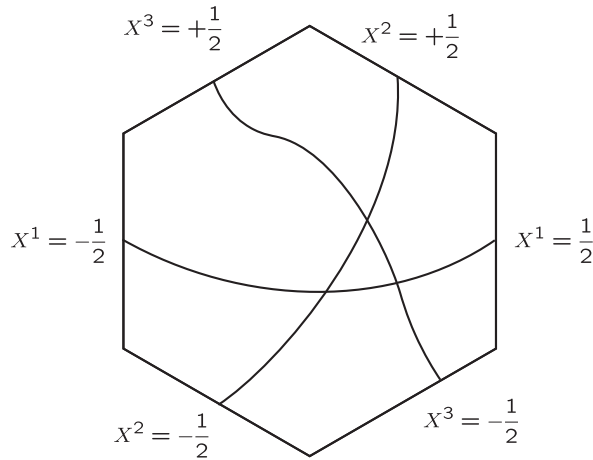


**Figure 18:** The length parameters  $X^1, X^2$ , and  $X^3$  along geodesics in classes  $C_1, C_2$ , and  $C_3$  respectively. The parameter  $X^\alpha$  attains the value  $-\frac{1}{2}$  on the edge  $e_\alpha$  and  $+\frac{1}{2}$  on the edge  $\tilde{e}_\alpha$ .

Our program gives a numerical solution for  $\phi^\alpha$  everywhere on the hexagon and hence the functions  $X^1, X^2, X^3$  can also be computed everywhere on the hexagon, described with fiducial coordinates  $(x, y)$ . The interpretation of  $X^\alpha$  as the length parameter, however, only holds in the region where the corresponding band of geodesics  $C_\alpha$  exists. In relating our results to Calabi's, we will focus on regions of the hexagon where the geodesics in class  $C_1$  and  $C_2$  exist. We shall use the length parameters  $(X^1, X^2)$  along geodesics in these two bands as coordinates.

Our convex program gives the extremal metric on  $P_6$  in the original fiducial coordinates  $(x, y)$ :

$$dA = \rho^2(x, y) dx \wedge dy. \quad (8.15)$$

Given the  $X^\alpha(x, y)$ , as well as the alternative area form  $dA = \frac{1}{\sqrt{1-f^2}} dX^1 \wedge dX^2$ , with  $f$  given in (8.6), we must have:

$$dA = \frac{1}{\sqrt{1-f^2}} \left| \frac{\partial(X^1, X^2)}{\partial(x, y)} \right| dx \wedge dy = \tilde{\rho}^2(x, y) dx \wedge dy. \quad (8.16)$$

The  $\tilde{\rho}$  so determined in the Riemannian language must coincide with the conformally determined  $\rho$  in the region  $U_3$ . Of course, since we are using our conformal data throughout, this is just a consistency check. Our data is not good enough to test that  $Z(X, Y)$  satisfies the differential equation (8.12) following from the variational principle.

Our numerical data can be used to compute the local angle  $\theta_{12}$  between geodesics. Using the conformal metric, we have

$$\cos \theta_{12} = \langle dX^1, dX^2 \rangle = \rho^{-2} \left( \frac{\partial X^1}{\partial x} \frac{\partial X^2}{\partial x} + \frac{\partial X^1}{\partial y} \frac{\partial X^2}{\partial y} \right). \quad (8.17)$$

The angle can also be computed from the Riemannian approach (8.3) as  $\sin \tilde{\theta}_{12} = \sqrt{1-f^2}$ , valid in the region where the geodesic band associated with  $Z$  exists. We expect agreement  $\theta_{12} = \tilde{\theta}_{12}$  in  $U_3$ .

Figure 19 shows  $\rho^2$  in blue and  $\tilde{\rho}^2$  in red along the hypotenuse of  $T_6$  parameterized with the fiducial distance  $r = \sqrt{x^2 + y^2}$ . This line runs from the center of the hexagon to the corner whose

neighborhood is covered by the first and second geodesic bands, but not the third. As would be expected, we find excellent agreement until we cross the transition point where  $U_3$  ends along this line. The transition point is the kink in the graph which occurs at  $r \simeq 0.49$ . This kink signals line curvature singularity as expected on the boundary of  $U_3$ . As expected, there is no agreement beyond  $U_3$ . (The maximum euclidean distance along this hypotenuse is 0.577.)

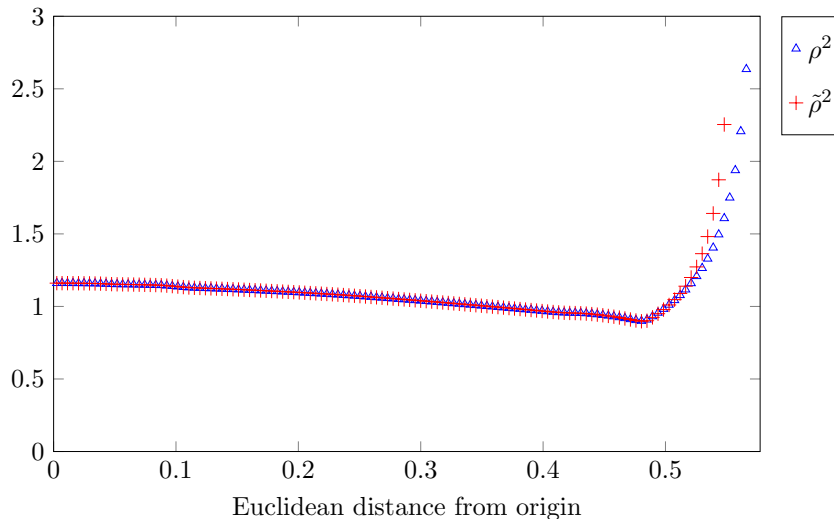


**Figure 19:** The conformal metric  $\rho^2$  (blue) and the alternative  $\tilde{\rho}^2$  (red) from the Riemannian computation. Both plotted along the hypotenuse of  $T_6$  and agreeing until the end of the  $U_3$  region at  $r \simeq 0.49$ .

Figure 20 shows two evaluations of the local angle between geodesics of the first and second classes along the diagonal of  $T_6$ :  $\theta_{12}$  (conformal, in blue) and  $\tilde{\theta}_{12}$  (Riemannian, in red). The boundary of  $U_3$  on the diagonal of  $T_6$  occurs when the angle  $\theta_{12}$  reaches  $\pi/2$ , consistent with a continuous transition into  $U_2$  where systolic bands must be orthogonal. Beyond this point the Riemannian determination is not valid, while the conformal one remains valid and relatively constant at  $\pi/2$  until one approaches the corner, where numerical errors become large. Consistent with the previous figure, the transition point is reached at about  $r \simeq 0.49$ .

### 8.3 Comments on a suggested extension for multiple bands

Following some remarks in [13], reference [17] investigated Calabi's variational principle and considered the equations that would apply for a region  $U_m$  covered by exactly  $m > 3$  bands of geodesics. Choosing potential functions  $(X, Y) \equiv (X^1, X^2)$  as coordinates on  $U_m$ , one has functions  $Z^i(X, Y)$  for  $i = 1, \dots, m-2$  for the remaining systolic bands. As we have seen, the condition that  $dZ^i$  is of unit norm determines the cotangent metric  $g^{-1}$

$$g^{-1} = \begin{pmatrix} 1 & f \\ f & 1 \end{pmatrix}, \quad f = \frac{1 - (Z_X^i)^2 - (Z_Y^i)^2}{2Z_X^i Z_Y^i}. \quad (8.18)$$

Since the metric is unique, all  $Z^i$  with  $i = 1, \dots, m-2$  must give the same value of  $f$ . In this proposal the Lagrangian  $L$  is not changed from (8.8), one simply demands that the equation of motion for  $Z(X, Y)$  have  $m-2$  inequivalent solutions  $Z^i(X, Y)$ , each of which gives the same  $f$  above. Since the

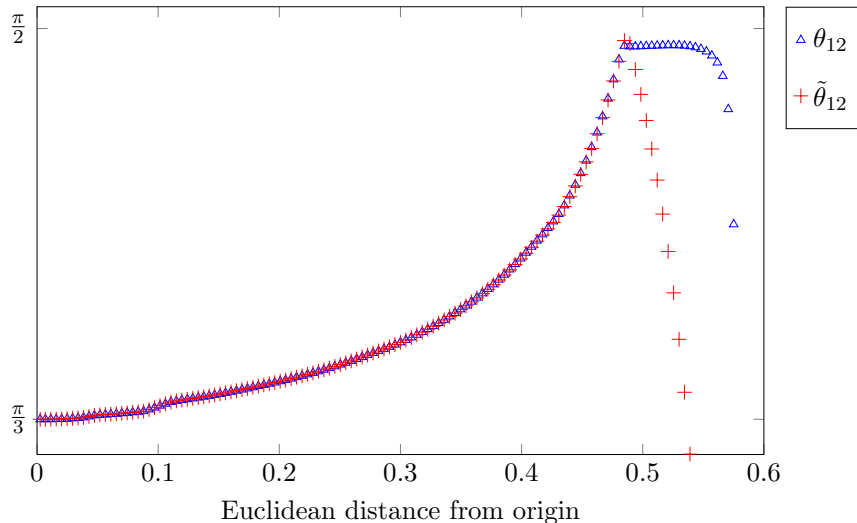


**Figure 20:** The local angle between the first and second bands of geodesics plotted along the hypotenuse of  $T_6$ :  $\theta_{12}$  (conformal, in blue) and  $\tilde{\theta}_{12}$  (Riemannian, in red). As expected, we see agreement until the angle reaches  $\frac{\pi}{2}$  at  $r \simeq 0.49$ , where  $U_3$  ends, and no agreement beyond this point.

Lagrangian is itself just a function of  $f$ , all solutions evaluate to the same Lagrangian. It was claimed in [17] that for any non-constant  $L$ , there are at most two inequivalent solutions to this prescribed Lagrangian problem and concluded that regions with five or more geodesics are necessarily flat. We are unable to confirm such variational principle for  $U_m$  with  $m > 3$ . Our proposal, given in section 9, makes use of Lagrange multipliers to implement the constraint of a single  $f$ , and ends up modifying the equation of motion of the  $Z^i$ .

In the rest of this section we point out a difficulty with the proposal of [17]. We consider the minimal area metric on  $\mathbb{RP}_2$ , a metric with an infinite number of bands of systolic geodesics. Not only is the extremal metric not flat, we can find the general  $Z^i(X, Y)$  that describes the geodesic bands that leads to a single  $f$ . This  $Z^i$ , however, does not satisfy the suggested equation of motion [17].

We choose the potentials  $X = x_0$  and  $Y = x_{\pi/2}$  as coordinates on the hemisphere. These are the potentials for the geodesic bands that originate at  $\phi = 0$  and at  $\phi = \pi/2$  and travel to the antipodal points. Using (7.16), they are given by

$$\begin{aligned} X(\theta, \phi) &= \frac{1}{\pi} \cos^{-1}(\sin \theta \cos \phi), \\ Y(\theta, \phi) &= \frac{1}{\pi} \cos^{-1}(\sin \theta \sin \phi). \end{aligned} \tag{8.19}$$

It follows that

$$\begin{aligned} \cos \pi X &= \sin \theta \cos \phi, \\ \cos \pi Y &= \sin \theta \sin \phi. \end{aligned} \tag{8.20}$$

The ranges of the coordinates  $X, Y$  can be determined (although they play no role in the calculation that follows). It turns out that the condition  $\sin^2 \theta = \cos^2 \pi X + \cos^2 \pi Y$  following from the two equations above imply that the subdomain  $D$  of  $X, Y \in [0, 1]$  that describes the hemisphere is the set of values for which  $\cos^2 \pi X + \cos^2 \pi Y \leq 1$ . The domain  $D$  is in fact the square formed by the midpoints of the edges in the unit square.

Starting from the round extremal metric on the hemisphere:

$$ds^2 = \frac{1}{\pi^2}(d\theta^2 + \sin^2 \theta d\phi^2), \quad (8.21)$$

a short calculation shows that in  $(X, Y)$  coordinates the components of the cotangent metric are

$$g^{XX} = g^{YY} = 1, \quad g^{XY} = -\cot \pi X \cot \pi Y. \quad (8.22)$$

We can now consider an arbitrary band departing from  $\phi = \phi_0$  and with potential  $Z^{\phi_0} = x_{\phi_0}$ . Using (7.16) we have:

$$Z^{\phi_0}(\theta, \phi) = \frac{1}{\pi} \cos^{-1}(\sin \theta \cos(\phi - \phi_0)). \quad (8.23)$$

Therefore

$$\cos \pi Z^{\phi_0} = \sin \theta \cos(\phi - \phi_0) = \sin \theta \cos \phi \cos \phi_0 + \sin \theta \sin \phi \sin \phi_0 \quad (8.24)$$

and using the earlier results we get

$$\cos \pi Z^{\phi_0} = (\cos \pi X) \cos \phi_0 + (\cos \pi Y) \sin \phi_0 \quad (8.25)$$

This defines the function  $Z^{\phi_0}(X, Y)$ . We now verify that for all values of  $\phi_0$ ,  $Z^{\phi_0}$  leads to the same  $f$  that happens to be equal to  $g^{XY}$ . Indeed, taking derivatives of (8.25) one quickly finds

$$Z_X^{\phi_0} = \frac{\sin \pi X}{\sin \pi Z^{\phi_0}} \cos \phi_0, \quad Z_Y^{\phi_0} = \frac{\sin \pi Y}{\sin \pi Z^{\phi_0}} \sin \phi_0. \quad (8.26)$$

A short calculation then gives

$$f = \frac{1 - (Z_X^{\phi_0})^2 - (Z_Y^{\phi_0})^2}{2Z_X^{\phi_0} Z_Y^{\phi_0}} = -\cot \pi X \cot \pi Y = g^{XY}. \quad (8.27)$$

As expected, the  $\phi_0$  dependence drops out. This confirms the consistency of the setup: after choosing two foliations to define coordinates on the surface, any additional foliation can be used to define the metric completely, providing the off-diagonal element.

On the other hand, this does not guarantee that  $Z^{\phi_0}(X, Y)$  solves the differential equation (8.12) associated to the Lagrangian  $L$ . The Lagrangian  $L$  at the extremum must coincide with the volume form, but this does not guarantee that the chosen Lagrangian is correct. To verify this we compute second partial derivatives.

$$\begin{aligned} Z_{XX}^{\phi_0} &= \left( \frac{\cos \pi X}{\sin \pi Z^{\phi_0}} - \sin^2 \pi X \frac{\cos \pi Z^{\phi_0}}{\sin^3 \pi Z^{\phi_0}} \cos \phi_0 \right) \pi \cos \phi_0, \\ Z_{XY}^{\phi_0} &= - \left( \sin \pi X \sin \pi Y \frac{\cos \pi Z^{\phi_0}}{\sin^3 \pi Z^{\phi_0}} \right) \pi \cos \phi_0 \sin \phi_0, \\ Z_{YY}^{\phi_0} &= \left( \frac{\cos \pi Y}{\sin \pi Z^{\phi_0}} - \sin^2 \pi Y \frac{\cos \pi Z^{\phi_0}}{\sin^3 \pi Z^{\phi_0}} \sin \phi_0 \right) \pi \sin \phi_0. \end{aligned} \quad (8.28)$$

Evaluating the left-hand side of (8.12) at various points we see that it does not vanish, and therefore the differential equation is not satisfied by  $Z^{\phi_0}$ . This can also be seen with modest effort by a perturbative analysis near the north pole of the sphere for a choice  $\phi_0 = \pi/4$  as we demonstrate now. Near the north pole we have  $X = Y = \frac{1}{2}$ . We do a change of variable  $X \rightarrow X + \frac{1}{2}, Y \rightarrow Y + \frac{1}{2}$ . We want to evaluate the left-hand side of equation (8.12) to first order in  $X$  and  $Y$ . We start by perturbatively expanding  $Z^{\pi/4}(X, Y)$  near the north pole to cubic order in coordinates

$$Z^{\pi/4}(X, Y) = \frac{1}{2} + \frac{X + Y}{\sqrt{2}} + \frac{\pi^2 XY (X + Y)}{4\sqrt{2}} + \dots \quad (8.29)$$

From this one readily computes various partial derivatives of  $Z(X, Y)$ :

$$\begin{aligned} Z_X^{\pi/4} &= \frac{1}{\sqrt{2}} + \frac{\pi^2}{4\sqrt{2}}Y(2X + Y) , & Z_Y^{\pi/4} &= \frac{1}{\sqrt{2}} + \frac{\pi^2}{4\sqrt{2}}X(X + 2Y) , \\ Z_{XX}^{\pi/4} &= \frac{\pi^2 Y}{2\sqrt{2}} , & Z_{XY}^{\pi/4} &= \frac{\pi^2(X + Y)}{2\sqrt{2}} , & Z_{YY}^{\pi/4} &= \frac{\pi^2 X}{2\sqrt{2}} . \end{aligned} \quad (8.30)$$

From this we compute various functions appearing in the EoM. To leading order, we have

$$f\left(Z_X^{\pi/4}, Z_Y^{\pi/4}\right) = \tilde{f}\left(Z_X^{\pi/4}, Z_Y^{\pi/4}\right) = \frac{1}{2} + \mathcal{O}(X^2) \quad g\left(Z_X^{\pi/4}, Z_Y^{\pi/4}\right) = 1 + \mathcal{O}(X^4) . \quad (8.31)$$

The left-hand side of the equation of motion (8.12) then evaluates to

$$\frac{3\pi^2(X + Y)}{4\sqrt{2}} \neq 0, \quad (8.32)$$

explicitly demonstrating that the equation is not satisfied. We will see in the following section that the modified variational principle gives an equation that is satisfied by the potentials in the  $\mathbb{RP}_2$  extremal metric.

## 9 Isosystolic variational principle with multiple foliations

We propose here a variational principle to determine the extremal minimal area Riemannian in a region  $U_m$  covered by  $m$  bands of systolic geodesics. For the case  $m = 3$  the answer was provided by Calabi [13]. We provide here a variational principle that works for  $m \geq 3$ , and differs from the proposal in [17] for  $m > 3$ .

After introducing this modified variational approach, we apply it to the extremal Riemannian metric in  $\mathbb{RP}_2$ , showing that the equations of motion following from the variational principle are satisfied. The computations are somewhat analogous to those that showed that the extremal metric in  $\mathbb{RP}_2$  satisfy the equations of the dual convex program.

### 9.1 Extension of the variational principle

Assume that we have a region  $U_m$  which is covered by exactly  $m \geq 3$  bands of geodesics. We choose any two geodesics potential functions  $X$  and  $Y$  as coordinates on  $U_m$  and express the remaining others as functions  $Z^i(X, Y)$ , with  $i = 1, \dots, m - 2$ . With cotangent space metric  $g^{XX} = g^{YY} = 1$  (to guarantee  $|dX| = |dY| = 1$ ) and  $g^{XY} \equiv f$ , to enforce the constraints  $|dZ^i| = 1$  for all  $i$  we require Lagrange multipliers  $\lambda_i$ . We thus have the variational principle:

$$I = \int dXdY \frac{1}{\sqrt{1-f^2}} \left( 1 + \sum_i \lambda_i \left[ (Z_X^i)^2 + (Z_Y^i)^2 + 2fZ_X^i Z_Y^i - 1 \right] \right). \quad (9.1)$$

Here  $f, \lambda_i$ , and  $Z^i$  must be viewed as functions of  $X$  and  $Y$  and are all to be varied to find stationary points of the functional  $I$ . As usual  $Z_X^i = \partial_X Z^i$  and  $Z_Y^i = \partial_Y Z^i$ .

The equations of motion for the Lagrange multipliers  $\lambda_i$  are:

$$(Z_X^i)^2 + (Z_Y^i)^2 + 2fZ_X^i Z_Y^i - 1 = 0 , \quad i = 1, \dots, n - 2. \quad (9.2)$$

Indeed this sets  $f$  equal to the desired value

$$f = \frac{1 - (Z_X^i)^2 - (Z_Y^i)^2}{2Z_X^i Z_Y^i}, \quad (9.3)$$

and makes the determination of  $f$  from each of the bands equal. Moreover, when this holds for all  $i$  the action  $I$  reduces to the integral of the area form (see (8.7)). The variation of  $f$  gives an equation of motion that using (9.2) becomes

$$\frac{f}{1-f^2} + 2 \sum_i \lambda_i Z_X^i Z_Y^i = 0. \quad (9.4)$$

Finally, the variation of  $Z^i$  gives the equation of motion

$$\partial_X \left[ \frac{\lambda_i}{\sqrt{1-f^2}} (Z_X^i + f Z_Y^i) \right] + \partial_Y \left[ \frac{\lambda_i}{\sqrt{1-f^2}} (Z_Y^i + f Z_X^i) \right] = 0. \quad (9.5)$$

Recalling that

$$g^{-1} = \begin{pmatrix} 1 & f \\ f & 1 \end{pmatrix}, \quad \sqrt{g} = \frac{1}{\sqrt{1-f^2}}, \quad (9.6)$$

and letting  $\mu, \nu$  indices run over  $X, Y$ , the last equation can be written covariantly as

$$\partial_\mu (\lambda_i \sqrt{g} g^{\mu\nu} \partial_\nu Z^i) = 0. \quad (9.7)$$

Using differential form notation the equation reads

$$d * (\lambda_i dZ^i) = 0. \quad (9.8)$$

Evaluating the derivatives in (9.5) and collecting terms we find a more explicit form of the  $Z^i$  equation of motion:

$$\begin{aligned} 0 = & Z_{XX}^i + Z_{YY}^i + 2f Z_{XY}^i \\ & + Z_X^i \left( \frac{\lambda_{iX} + f \lambda_{iY}}{\lambda_i} + \frac{f_Y + f f_X}{1-f^2} \right) + Z_Y^i \left( \frac{\lambda_{iY} + f \lambda_{iX}}{\lambda_i} + \frac{f_X + f f_Y}{1-f^2} \right). \end{aligned} \quad (9.9)$$

It is straightforward to verify that for  $n = 3$  the new equations of motion are equivalent to those of [13, 17], which we reviewed in 8.1.

## 9.2 Extremal Riemannian metric on $\mathbb{RP}_2$ from new variational principle

In this section we show that the extremal Riemannian metric on  $\mathbb{RP}_2$  satisfies the Euler-Lagrange equations obtained from the new variational principle. We begin with some preliminary discussion of equation (9.8),

$$d * (\lambda_i dZ^i) = 0. \quad (9.10)$$

This is very similar to the equation of motion derived using conformal methods (see discussion after eq. (7.19) of [14]). In that notation we had

$$u^\alpha = - \frac{*d\varphi^\alpha}{|d\varphi^\alpha|}, \quad (9.11)$$

with the local metric taking the form

$$ds^2 = (dx^\alpha)^2 + \frac{1}{h_\alpha^2} (d\varphi^\alpha)^2. \quad (9.12)$$

It follows that  $|d\varphi^\alpha| = |h_\alpha|$ , where  $h_\alpha$  has the interpretation of the density of  $\alpha$  geodesics. In fact,  $\varphi^\alpha$  are the functions that appear in the dual program and are constants along  $\alpha$ -geodesics. We also note that  $u^\alpha = dx^\alpha$  where  $x^\alpha$  is the length parameter along  $\alpha$ -geodesics. Therefore (9.11) and  $*(*u) = -u$ , gives

$$d\varphi^\alpha = *(|h_\alpha| dx^\alpha). \quad (9.13)$$

Taking another exterior derivative we get

$$d * (|h_\alpha| dx^\alpha) = 0. \quad (9.14)$$

We verified this equation explicitly in section 7 where we showed that the metric on  $\mathbb{RP}_2$  was a solution of the dual (conformal) program. This equation is exactly analogous to equation (9.10) with the Lagrange multipliers identified with the functions that determine geodesic density. The  $Z^{\phi_0}$  in (8.23) are in fact length coordinates of the  $x^\alpha$  type. As before  $\phi_0$  is the label for a systolic band. In this language we would have a metric defined via the band:

$$ds^2 = (dZ^{\phi_0})^2 + \frac{1}{\tilde{h}_{\phi_0}^2} (d\tilde{\varphi}_{\phi_0})^2. \quad (9.15)$$

It follows that if we choose  $\lambda_{\phi_0} \sim |\tilde{h}_{\phi_0}|$  with  $|\tilde{h}_{\phi_0}|$  given in equation (7.36) then the equation of motion (9.10), reading now  $d * (\lambda_{\phi_0} dZ^{\phi_0}) = 0$  is guaranteed to be satisfied. We will anyway check the equation explicitly.

We note, however, the analog of a reparameterization ambiguity discussed around (7.5) for the dual-program analysis of the  $\mathbb{RP}_2$  metric. If a pair  $(\lambda_i, Z^i)$  satisfies equation (9.7) then a pair

$$(\chi(\varphi^i) \lambda_i, Z^i), \quad (9.16)$$

with a rescaled  $\lambda_i$  will also satisfy the equation if

$$g^{\mu\nu} \partial_\mu Z^i \partial_\nu \varphi^i = 0. \quad (9.17)$$

But this holds when  $(Z^i, \varphi^i)$  are a pair of orthonormal coordinates for a systolic band. In our case, the coordinate pair is  $(Z^{\phi_0}, \tilde{\varphi}_{\phi_0})$  and the metric (9.15) indeed implies that

$$0 = \langle dZ^{\phi_0}, d\tilde{\varphi}_{\phi_0} \rangle = g^{\mu\nu} \partial_\mu Z^{\phi_0} \partial_\nu \tilde{\varphi}_{\phi_0}. \quad (9.18)$$

We thus have the freedom to replace solutions as

$$(\lambda_{\phi_0}, Z^{\phi_0}) \rightarrow (\chi(\tilde{\varphi}_{\phi_0}) \lambda_{\phi_0}, Z^{\phi_0}). \quad (9.19)$$

To confirm that we have a solution for the extremal metric on  $\mathbb{RP}_2$  we consider an arbitrary systolic band departing from  $\phi = \phi_0$  for which the length parameter  $Z^{\phi_0}$  is given in equation (8.25):

$$\cos \pi Z^{\phi_0} = (\cos \pi X) \cos \phi_0 + (\cos \pi Y) \sin \phi_0. \quad (9.20)$$

We also recall that the extremal metric has (8.27):

$$f = -\cot \pi X \cot \pi Y. \quad (9.21)$$

These two,  $Z^{\phi_0}$  and  $f$ , with values so specified must solve the equations of motion. The only unknown is the value of the Lagrange multipliers  $\lambda_{\phi_0}$ . From the above remarks, however, we can choose  $\lambda_{\phi_0}$  equal to the first choice  $\tilde{h}$  in (7.36):

$$\lambda_{\phi_0} = \frac{1}{\sin \pi Z^{\phi_0}}, \quad (9.22)$$

keeping in mind that we are free to multiply it with an arbitrary function of  $\tilde{\varphi}_{\phi_0}$ . Our task now is to verify explicitly that we have a solution, and in doing so we will find the final form of  $\lambda_{\phi_0}$ .

The equation of motion for  $Z^{\phi_0}$  is (9.9), with  $i \rightarrow \phi_0$ . With a little reordering it reads:

$$\begin{aligned} 0 = & Z_{XX}^{\phi_0} + Z_{YY}^{\phi_0} + 2f Z_{XY}^{\phi_0} + \frac{1}{\lambda_{\phi_0}} \left( Z_X^{\phi_0} (\lambda_{\phi_0 X} + f \lambda_{\phi_0 Y}) + Z_Y^{\phi_0} (\lambda_{\phi_0 Y} + f \lambda_{\phi_0 X}) \right) \\ & + \frac{1}{1-f^2} \left[ f_X \left( Z_Y^{\phi_0} + f Z_X^{\phi_0} \right) + f_Y \left( Z_X^{\phi_0} + f Z_Y^{\phi_0} \right) \right]. \end{aligned} \quad (9.23)$$

We now claim that for  $Z^{\phi_0}$  the first three terms in the above equation add up to zero:

$$Z_{XX}^{\phi_0} + Z_{YY}^{\phi_0} + 2f Z_{XY}^{\phi_0} = 0. \quad (9.24)$$

This is readily verified with a bit of work using the second derivatives computed in (8.28). Since  $\lambda_{\phi_0}$  is just a function of  $Z^{\phi_0}$ , using chain rule we quickly see that

$$\begin{aligned} \frac{1}{\lambda_{\phi_0}} \left( Z_X^{\phi_0} (\lambda_{\phi_0 X} + f \lambda_{\phi_0 Y}) + Z_Y^{\phi_0} (\lambda_{\phi_0 Y} + f \lambda_{\phi_0 X}) \right) &= \frac{1}{\lambda_{\phi_0}} \frac{d\lambda}{dZ^{\phi_0}} [(Z_X^{\phi_0})^2 + (Z_Y^{\phi_0})^2 + 2f Z_X^{\phi_0} Z_Y^{\phi_0}] \\ &= \frac{1}{\lambda_{\phi_0}} \frac{d\lambda}{dZ^{\phi_0}} = -\pi \cot \pi Z^{\phi_0}. \end{aligned} \quad (9.25)$$

In passing to the second line we recalled that the expression in brackets is  $|dZ^{\phi_0}|^2 = 1$ . The equation of motion has thus simplified to

$$0 = -\pi \cot \pi Z^{\phi_0} + \frac{1}{1-f^2} \left[ f_X \left( Z_Y^{\phi_0} + f Z_X^{\phi_0} \right) + f_Y \left( Z_X^{\phi_0} + f Z_Y^{\phi_0} \right) \right]. \quad (9.26)$$

We use the first derivatives (8.26) to compute:

$$\begin{aligned} f_X \left( Z_Y^{\phi_0} + f Z_X^{\phi_0} \right) &= \frac{\pi \cos \pi Y}{\sin \pi Z^{\phi_0} \sin \pi X \sin \pi Y} \left( \frac{\sin \pi Y}{\sin \pi X} \sin \phi_0 - \cot \pi X \cot \pi Y \cos \phi_0 \right), \\ f_Y \left( Z_X^{\phi_0} + f Z_Y^{\phi_0} \right) &= \frac{\pi \cos \pi X}{\sin \pi Z^{\phi_0} \sin \pi X \sin \pi Y} \left( \frac{\sin \pi X}{\sin \pi Y} \cos \phi_0 - \cot \pi X \cot \pi Y \sin \phi_0 \right). \end{aligned} \quad (9.27)$$

Adding above two terms and simplifying we find

$$\begin{aligned} f_X \left( Z_Y^{\phi_0} + f Z_X^{\phi_0} \right) + f_Y \left( Z_X^{\phi_0} + f Z_Y^{\phi_0} \right) &= \pi \cot \pi Z^{\phi_0} (1 - \cot^2 \pi X \cot^2 \pi Y) \\ &= \pi \cot \pi Z^{\phi_0} (1 - f^2). \end{aligned} \quad (9.28)$$

Back in (9.26) we have a complete cancellation. This completes the verification that the equation of motion for  $Z^{\phi_0}$  is satisfied.

We now verify the equation of motion for  $f$ , given in (9.4) and rearranged as follows:

$$2 \frac{1-f^2}{f} \sum_{\phi_0} \lambda_{\phi_0} Z_X^{\phi_0} Z_Y^{\phi_0} = -1. \quad (9.29)$$



Multiplying by  $\Delta\phi_0 = \pi/n$ , for the case of  $n$  systolic bands, with  $n$  large, we turn the left-hand side into an integral:

$$2 \frac{1-f^2}{f} \int_0^\pi d\phi_0 \lambda_{\phi_0} Z_X^{\phi_0} Z_Y^{\phi_0} = -\frac{\pi}{n}. \quad (9.30)$$

It is easiest to verify the equation in fiducial disk coordinates  $(x, y)$  using the parameters  $a$  and  $b$  defined in equation (7.42). These different representations are obtained by straightforward computations, using the expressions for  $X, Y$ , and  $Z$  in terms of  $(x, y)$  given in (7.18). We first consider separately the various ingredients of the above left-hand side. For the prefactor,

$$\begin{aligned} \frac{1-f^2}{f} &= \cot(\pi X) \cot(\pi Y) - \tan(\pi X) \tan(\pi Y) \\ &= -\frac{(1-16|z|^4)^2}{16xy\sqrt{(1-16|z|^4)^2 + 256x^2y^2}} = -\frac{1-a^2-b^2}{b\sqrt{1-a^2}}. \end{aligned} \quad (9.31)$$

We now consider  $\lambda_{\phi_0}$ , already given in (9.22). Recall that we are free to scale  $\lambda_{\phi_0}$  by an arbitrary function which is constant along  $\phi_0$ -geodesics without spoiling the equation of motion for  $Z^{\phi_0}$ . We choose to make  $\lambda_{\phi_0}$  proportional to  $|h_{\phi_0}|$  in equation (7.40). For this we multiply our original choice by  $\cos \tilde{\varphi}_{\phi_0}$  and a constant  $\beta$  to be determined:

$$\lambda_{\phi_0} = \beta |h_{\phi_0}| = \beta \frac{\cos \tilde{\varphi}_{\phi_0}}{\sin(\pi Z^{\phi_0})}. \quad (9.32)$$

Recall that  $\tilde{\varphi}_{\phi_0}$  in disk coordinates is given in (7.24) and is, by construction, constant along  $\phi_0$ -geodesics. In terms of the disk coordinates and parameters  $a$  and  $b$  we have

$$\lambda_{\phi_0} = \frac{\beta(1-16|z|^4)}{1+16|z|^4-8(x^2-y^2)\cos 2\phi_0-16xy\sin 2\phi_0} = \frac{\beta\sqrt{1-a^2-b^2}}{1-a\cos 2\phi_0-b\sin 2\phi_0}. \quad (9.33)$$

We now evaluate the product  $Z_X^{\phi_0} Z_Y^{\phi_0}$ , beginning with equation (8.26):

$$\begin{aligned} Z_X^{\phi_0} Z_Y^{\phi_0} &= \frac{\sqrt{(1+16|z|^4)^2 + 256x^2y^2} \sin 2\phi_0}{2(1+16|z|^4-8(x^2-y^2)\cos 2\phi_0-16xy\sin 2\phi_0)}, \\ &= \frac{\sqrt{1-a^2} \sin(2\phi_0)}{2(1-a\cos 2\phi_0-b\sin 2\phi_0)}. \end{aligned} \quad (9.34)$$

Collecting the above ingredients we now get:

$$2 \frac{1-f^2}{f} \lambda_{\phi_0} Z_X^{\phi_0} Z_Y^{\phi_0} = -\frac{\beta}{b} (1-a^2-b^2)^{3/2} \frac{\sin 2\phi_0}{(1-a\cos 2\phi_0-b\sin 2\phi_0)^2}. \quad (9.35)$$

We perform the integral required in (9.30):

$$-\frac{\beta}{b} (1-a^2-b^2)^{3/2} \int_0^\pi \frac{\sin 2\phi_0 d\phi_0}{(1-a\cos 2\phi_0-b\sin 2\phi_0)^2} = -\frac{\pi}{n}. \quad (9.36)$$

The integral can be evaluated by relating it to an already computed integral in (7.44):

$$\begin{aligned} \int_0^\pi \frac{\sin 2\phi_0 d\phi_0}{(1-a\cos 2\phi_0-b\sin 2\phi_0)^2} &= \frac{d}{db} \int_0^\pi \frac{d\phi_0}{(1-a\cos 2\phi_0-b\sin 2\phi_0)} \\ &= \frac{d}{db} \frac{\pi}{\sqrt{1-(a^2+b^2)}} = \frac{\pi b}{(1-a^2-b^2)^{3/2}}. \end{aligned} \quad (9.37)$$

Back in (9.36) all the position dependence cancels, showing that the equation is satisfied when the constant  $\beta$  is chosen to be

$$-\beta\pi = -\frac{\pi}{n} \quad \rightarrow \quad \beta = \frac{1}{n}. \quad (9.38)$$

This completes the verification that the extremal metric in  $\mathbb{RP}_2$  satisfies the Euler-Lagrange equations coming from the new variational principle.

## Acknowledgements

We are indebted to Matthew Headrick for his help in constructing the argument in section 2.2 and for conversations that led to the variational principle of section 9. We thank Michael Wolf for instructive discussions and Liam Cohen for discussions on triangulations at the very early stages of this work. This material is based upon work supported by the U.S. Department of Energy, Office of Science, Office of High Energy Physics of U.S. Department of Energy under grant Contract Number DE-SC0012567. U.N also acknowledges the fellowship by the Knut and Alice Wallenberg Foundation, Stockholm, Sweden.

## A Discretization of polygons for numerical analysis

### A.1 Hexagon

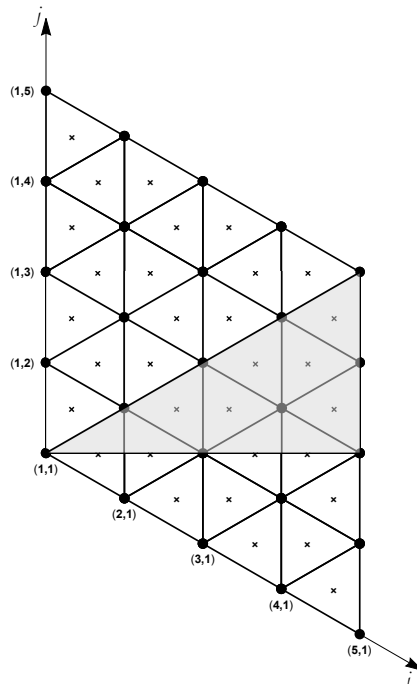


**Figure 21:** Discretization of the parallelogram for  $N_c = 4$ . The shaded region is the fundamental domain  $T_6$  discussed in section 2. The functions  $\phi^1$  and  $\varphi^1$  is defined at the vertices of plaquettes, denoted by ‘dots’. Their derivatives are evaluated at the centroid of each plaquette, denoted by a ‘cross’.

For the discretization of the hexagon the plaquettes are equilateral triangles that fit seamlessly into the parallelogram with vertices at  $(0, 0)$ ,  $(1, -\frac{1}{\sqrt{3}})$ ,  $(1, \frac{1}{\sqrt{3}})$  and  $(0, \frac{2}{\sqrt{3}})$ , as shown in Figure 21. We denote by  $N_c$  the number of plaquette edges on each side of the parallelogram. For any fixed  $N_c$ , the region is triangulated by  $2N_c^2$  plaquettes. The  $(i, j)$  labels at the corners of the plaquettes are based on axes running along the edges of the parallelogram. We have  $i, j = 1, \dots, N_c + 1$ . Figure 21 shows a discretization for  $N_c = 4$ .

As discussed in section 2, one only needs to use the region  $Q_6$  of the hexagon in the first quadrant as the fundamental region for the primal variable  $\phi^1$  and for the dual variable  $\varphi^1$ . Moreover, one effectively works with the region  $T_6$  (shaded on the figure) which is the fundamental domain of the metric. The functions  $\phi^\alpha$  and  $\varphi^\alpha$  are defined on the vertices of the plaquettes. Derivatives are defined at the centroid of each plaquette in terms of the value of the function at the vertices of the plaquette. In figure 21, centroids are marked by a  $\times$ . We label the centroids by  $[i, j]$  where  $i = 1, 2, \dots, N_c$  and  $j = 1, 2, \dots, 2N_c$  as shown in Figure 22.

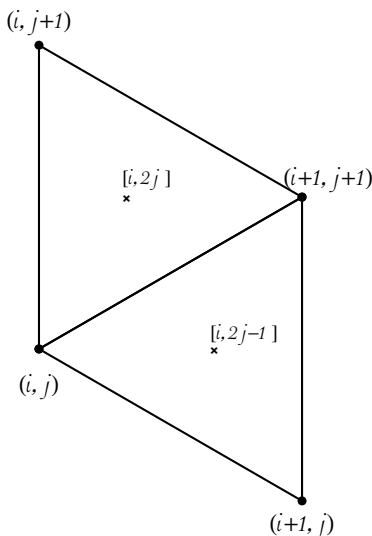


**Figure 22:** Labeling the centroids of plaquettes with two integers  $[\tilde{i}, \tilde{j}]$ . We use the left-lower vertex  $(i, j)$  to generate labels for two centroids. Both are assigned the value  $\tilde{i} = i$ . For the centroid to the right of the vertex  $(i, j)$  we assign  $\tilde{j} = 2j - 1$  and for the other  $\tilde{j} = 2j$ .

## A.2 Octagon and higher polygons

For any polygon  $P_{2n}$  with  $n \geq 4$ , we discretize the fundamental region  $T_{2n}$  using the same strategy: we discretize into smaller triangles *similar* to  $T_{2n}$ .  $N_c$  is the number of subdivisions of the apothem as well as the number of subdivisions of half of the polygon edge  $\tilde{e}_1$ . This gives  $N_c^2$  plaquettes on  $T_{2n}$  and  $nN_c^2$  plaquettes on  $Q_{2n}$ . Figure 23 shows the case  $N_c = 4$ , with  $T_{2n}$  shaded, and a copy of it immediately above, whose discretization is obtained by reflection across the hypotenuse of  $T_{2n}$ . These two triangles define the building block that is then successively rotated rigidly to provide a triangulation of  $Q_{2n}$ .

The functions  $\phi^\alpha$  and  $\varphi^\alpha$ , relevant to the primal and dual programs, respectively, are defined on the vertices of the triangular plaquettes. These vertices, over  $T_{2n}$ , are labelled by integers  $(i, j)$ , with  $i = 1, \dots, N_c + 1$  and  $j = 1, \dots, i$ . To extend the labeling over  $Q_{2n}$  one can simply let  $j$  run

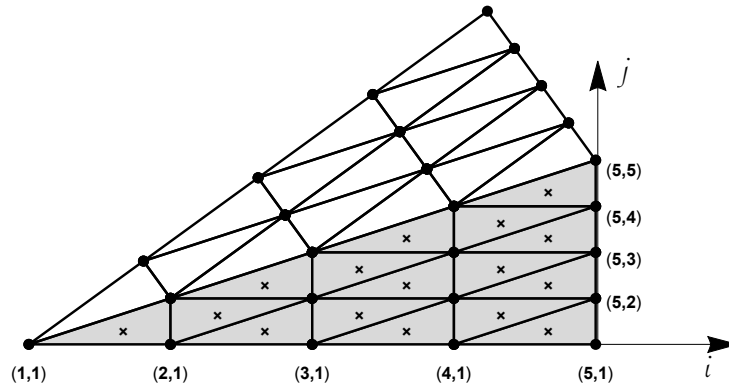


**Figure 23:** Discretization scheme for  $P_{2n}$  with  $N_c = 4$  subdivisions of the apothem. The shaded region denotes the fundamental triangle  $T_{2n}$ . Each triangular plaquette is *similar* to  $T_{2n}$ . Functions  $\phi^\alpha$  and  $\varphi^\alpha$  are defined on vertices of plaquettes and their derivatives are defined on centroids. The triangulation is extended across the hypotenuse of  $T_{2n}$  by reflection.

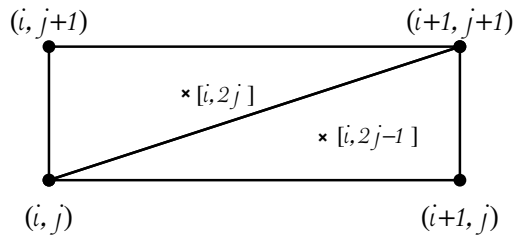


**Figure 24:** Labeling the vertices and centroids of triangular plaquettes. As in the case of the hexagon, the left-lower vertex  $(i, j)$  is used to label centroids of two triangles. The centroid of the lower triangle is labeled  $[i, 2j - 1]$  and the centroid of the upper triangle is labeled  $[i, 2j]$ .

over a larger set of integers. Derivatives are calculated at the *centroids* of the triangular plaquettes, marked by  $\times$ . These points are labelled by two integers  $[i, j]$ , as explained in Figure 24. These integers take values  $i = 1, 2, \dots, N_c$  and  $j = 1, 2, \dots, 2i - 1$ .

## References

- [1] K. Strebel, *Quadratic differentials*, Springer-Verlag Berlin Heidelberg 1984.
- [2] L. V. Ahlfors, *Conformal Invariants: Topics in Geometric Function Theory*, AMS Chelsea Publishing (1973).
- [3] B. Zwiebach, “How Covariant Closed String Theory Solves A minimal-area problem,” *Commun. Math. Phys.* **136**, 83 (1991). doi:10.1007/BF02096792
- [4] B. Zwiebach, “Closed string field theory: Quantum action and the B-V master equation,” *Nucl. Phys. B* **390**, 33 (1993) doi:10.1016/0550-3213(93)90388-6 [hep-th/9206084].
- [5] M. Wolf and B. Zwiebach, “The Plumbing of minimal area surfaces,” *Journal of Geometry and Physics* **15** (1994) 23-56. [hep-th/9202062].
- [6] M. Gromov, “Filling Riemannian Manifolds,” *J. Differential Geom.* **18** (1983) 1-147.
- [7] M. G. Katz, *Systolic Geometry and Topology*, Mathematical Surveys and Monographs, Volume 137. American Mathematical Society 2007.
- [8] M. Berger, “A Panoramic View of Riemannian Geometry,” Springer-Verlag Berlin Heidelberg 2003.
- [9] L. Guth, “Metaphors in systolic geometry”, arXiv:1003.4247. “Systolic inequalities and minimal hyper surfaces”, arXiv:0903.5299.
- [10] C. Bavard, “Inégalités isosystoliques conformes,” *Comment. Math. Helv.* **67** (1992) 146-166.
- [11] Mikhail Katz and Stéphane Sabourau, “An optimal systolic inequality for CAT(0) metrics in genus two.” *Pacific Journal of Mathematics*, vol. **227** (2006), no. 1, 95-107.
- [12] Mikhail Katz and Stéphane Sabourau, “Systolically extremal non positively curved surfaces are flat with finitely many singularities,” to appear.
- [13] E. Calabi, “Extremal isosystolic metrics for compact surfaces.” pp. 167-204 in *Actes de la Table Ronde de Géométrie Différentielle* (Luminy, 1992), Soc. Math. France, Paris, 1996.
- [14] M. Headrick and B. Zwiebach, “Convex programs for minimal-area problems,” arXiv:1806.00449 [hep-th].
- [15] M. Headrick and B. Zwiebach, “Minimal-area metrics on the Swiss cross and punctured torus,” arXiv:1806.00450 [hep-th].
- [16] S. Boyd and L. Vandenberghe, *Convex Optimization*, Cambridge University Press (2004). Available online at: <https://web.stanford.edu/~boyd/cvxbook/>
- [17] R. L. Bryant, “On extremals with prescribed Lagrangian densities,” in “Manifolds and Geometry” (Pisa, 1993), Cambridge University Press, 1996. arXiv:dg-ga/9406001.
- [18] P. M. Pu, “Some inequalities in certain nonorientable Riemannian manifolds”, *Pacific. J. Math.* **2** (1952) 55-71.